Technical Reports

CENTRO EURO-MEDITERRANEO
PER I CAMBIAMENTI CLIMATICI

ANS – Numerical Applications and Scenarios Division

EU-Japan Meeting on the Development of Next Generation Climate Models

ANS – Numerical Applications and Scenarios Division

Centro Euro-Mediterraneo
per i Cambiamenti Climatici
www.cmcc.it

December 2007 ■ TR4

EU-Japan Meeting on the Development of Next Generation Climate Models. 6-7 December 2006, Hotel Bauer, Venice

Summary

In this technical report we present the compilation of the abstract of the papers presented at the Joint EU-Japan meeting held in Venice, Dec 6-7, 2006.
The European groups and the Frontier group have been cooperating now for almost ten years. The cooperation has been developing exploiting a string of EU projects (SINTEX, ENSEMBLES, CIRCE, DYNAMITE) and national initiatives and centers, like the Max-Planck Institut in Hamburg and the newly established Euromediterranean Center for Climate Change (CMCC) in Italy. The cooperation has been a very fruitful one, several important results have been obtained, many papers have been published, but most importantly a lasting scientific relation has been established. The quasi-annual meetings have marked this advance and served as a checking point for the development of our joint science.

Keywords: Climate Variability, General Circulation Models.

JEL Classification:

Address for correspondence:
Enrico Scoccimarro
Istituto Nazionale di Geofisica e Vulcanologia
Via A. Moro, 44
40127 Bologna, Italy.
E-mail: scoccimarro@bo.ingv.it

**EU-Japan Meeting on the Development of
Next Generation Climate Models:**

Agenda

Wednesday 6 Dec.

14.00: Opening of the Meeting

- 14.05 **A. Navarra**: *Welcome*

Session 1: *Chair:* A. Navarra

- 14.15 **T. Yamagata** (FRCGC/JAMSTEC/U of Tokyo): *"The ENSO Modoki: Another Coupled Mode in the Tropical Pacific?"*
- 14.45 **H. Sakuma** (FRCGC/JAMSTEC): *"The Japanese initiatives for international collaborative studies on climate prediction."*
- 15.15 **J.-J. Luo** (FRCGC/JAMSTEC): *"Seasonal-to-interannual climate predictability in a fully coupled OAGCM."*

15.45-16.00: Coffee break

- 16.00 **C. Montégut** (FRCGC/JAMSTEC): *"Preliminary results from a new version of the SINTEX-F coupled model."*
- 16.30 **T. Tozuka** (Univ. of Tokyo): *"Ocean thermodynamics of the simulated ENSO: A seasonally stratified analysis using SINTEX-F CGCM results"*
- 17.00 **M. Nonaka** (FRCGC/JAMSTEC): *"Decadal variations of SST in the western North Pacific and associated atmospheric variations"*

17.30: Discussion

18.00: End of Day 1

20.30 Meeting dinner

<u>**Thursday 7 Dec.**</u>

8.55: Opening Day 2

Session 2: *Chair:* <u>E. Rockner</u>

- 9.00 **S. Behera** (FRCGC/JAMSTEC): *"The Intrinsic Indian Ocean Dipole and its impact on world weather and climate"*.
- 9.30 **K. Miyakoda** (GFDL): *"ENSO Oscillation- the biennial oscillation and the global warming"*
- 10.00 **A. Navarra** (CMCC): *"CIRCE: a climate change impacts in the Mediterranean"*

10.30 – 10.45: Coffee break

- 10.45 **E. Scoccimarro** (CMCC) : *"The INGV(CMCC) IPCC scenario simulations"*
- 11.15 **S. Gualdi** (CMCC): *"INGV(CMCC) IPCC scenario simulations: changes in the tropical climate"*
- 11.45 **A. Bellucci** (CMCC): *"Decadal Variability in the North Atlantic climate system"*

12.15: Discussion

12.45: Lunch

Session 3: *Chair:* <u>T. Yamagata</u>

- 14.00 **A. Alessandri** (CMCC): "*Land-Surface-Vegetation effects on climate: application to seasonal predictions*"
- 14.30 **A. Cherchi** (CMCC): *"The Sensitivity of the Indo-Pacific climate variability to model resolution and CO2 concentration"*
- 15.00 **E. Manzini** (CMCC): *"The INGV-CMCC Earth System Model: Preliminary results"*

15.30-15.45: Coffee break

- 15.45 **M. Vichi** (CMCC): *"Physical-Biogeochemical interactions across scales in the global ocean"*
- 16.15 **E. Rockner** (MPI-MET): *"Modelling the global atmosphere at high horizontal resolution"*
- 16.45 **M. Giorgetta** (MPI-MET): *"Intercomparison between climate and middle atmosphere models: Impacts of the stratospheric representation on the troposphere in AMIP simulations and on couplet AOGCM simulations"*
- 17.15 **S. Masson** (LODYC): *"Implementation of OPA9 in the SINTEX coupled model: new points and first results"*

17.45: Discussion
18.15: End of Meeting

Introduction

A.Navarra [1,2]

1 Istituto Nazionale di Geofisica e Vulcanologia, Bologna, Italy
2 Centro Euro-Mediterraneo per i Cambiamenti Climatici, Lecce, Italy

Climate science is at a very interesting juncture these days. The increasing social and political relevance of the findings and methods of our research to a decision process that will shape the development of the world in the coming decades is putting climate science and its practitioners in the limelight. The scientific debate has become often tangled with political agendas of various origin, sometimes lobbysts and activists from all parts of the political spectrum are trying to manipulate science and the scientists, sometimes it is some scientists that is trying to manipulate the media to gain some advantage.

Our community is going through a similar process to the one that shook the nuclear physicists community in the 40's and 50's when, according to a famous quote by Robert Oppenheimer,

> *In some sort of crude sense, which no vulgarity, no humor, no overstatement can quite extinguish, the physicists have known sin; and this is a knowledge which they cannot lose.*

Now climate scientists have also know sin and our work has become even more challenging and fascinating, resounding with overtones of social, economic and political issues that come together in an amazing bundle. We feel the responsibility and the burden of this knowledge. This complex tangle of disciplines and different dictionaries is now are daily working field, so it is particularly precious when we can take a step back and revert to a plain, simple, serene discussion on climate dynamics.

The European groups and the Frontier group have been cooperating now for almost ten years. The cooperation has been developing exploiting a string of EU projects (SINTEX, ENSEMBLES, CIRCE, DYNAMITE) and national initiatives and centers, like the Max-Planck Institut in Hamburg and the newly established Euromediterranean Center for Climate Change (CMCC) in Italy. The cooperation has been a very fruitful one, several important results have been obtained, many papers have been published, but most importantly a lasting scientific relation has been established. The quasi-annual meetings have marked this advance and served as a checking point for the development of our joint science.

The common work has contributed to advance our understanding in the climate variability of the Indo Pacific region and its connection to the extratropics, it has also shown the importance of a realistic tropical interannual variability for climate change simulations, a point somewhat overlooked in the popular climate scenario work.

It is therefore with great pleasure that we present the compilation of the abstract of the papers presented at the Joint EU-Japan meeting held in Venice, Dec 6-7, 2006.

El Niño Modoki (Pseudo-El Niño) and its Impact on the World Climate

T. Yamagata[1, 2],K. Ashok[1], S. Behera[1], S. Rao[1] and H. Weng[1]

1: Climate Variations Research Program (CVRP), Frontier Research Center for Global Change (FRCGC), Japan Agency for Marine-Earth Science and Technology (JAMSTEC), 3173-25 Showa-machi, Kanazawa-ku, Yokohama, Kanagawa 236-0001, Japan; Tel: 81-45-778-5502; Fax: 81-45-778-5707
2: Department of Earth and Planetary Science (DEPS), Graduate School of Science, The University of Tokyo, 7-3-1 Hongo, Bunkyo-ku, Tokyo 113-0033, Japan; Tel: 81-3-5841-4297; Fax: 81-3-5841-8791; E-mai: yamagata@eps.s.u-tokyo.ac.jp

Using various ocean/atmosphere datasets mainly for the period 1979-2005, we suggest the existence of a new climate mode that is different from conventional El Niño in the central tropical Pacific. The unique central Pacific warming is associated with a horse-shoe SST pattern, and is flanked by a colder anomaly on both sides along the equator (Fig. 1). Such a zonal SST distribution results in anomalous two-cell Walker circulations over the tropical Pacific (Fig. 2). Both ITCZ and SPCZ expand poleward, forming a wet region in the central tropical Pacific. Conventional EOF analysis of monthly tropical Pacific SSTA shows that the new mode is represented by the second mode that explains 12% of the variance.

Since the mode cannot be described as one phase of El Niño evolution, we suggest that the phenomenon should be called El Niño Modoki[1] (Pseudo-El Niño). The El Niño Modoki involves ocean-atmosphere coupled processes, indicating the existence of a unique atmospheric component during the evolution, which is analogous to the Southern Oscillation in case of El Niño. Thus the total entity should be called ENSO Modoki.

The Modoki's impact on the world climate is very different from that of ENSO (and IOD). Possible geographical regions for droughts and floods influenced by Modoki and ENSO are compared. Interestingly, the Modoki's influences over regions such as the Far East including Japan and the western coast of USA are almost opposite to those of the conventional ENSO (Fig. 3).

The difference maps between the two periods of 1979-2004 and 1958-1978 for various oceanic/atmospheric variables suggest that the recent weakening of equatorial easterlies related to weakened zonal sea surface temperature gradient led to more flattening of the thermocline. This appears to be a cause of more frequent and persistent occurrence of the Modoki event during recent warming decades; the ENSO Modoki has a large decadal background while ENSO is predominated by interannual variability.

[1] "Modoki" is a classical Japanese word, which means "a similar but different thing".

Appreciating the two different phenomena in the tropical Pacific will enhance our understanding of the coupled ocean-atmosphere dynamics and thus contribute to reducing the uncertainty in the climate prediction.

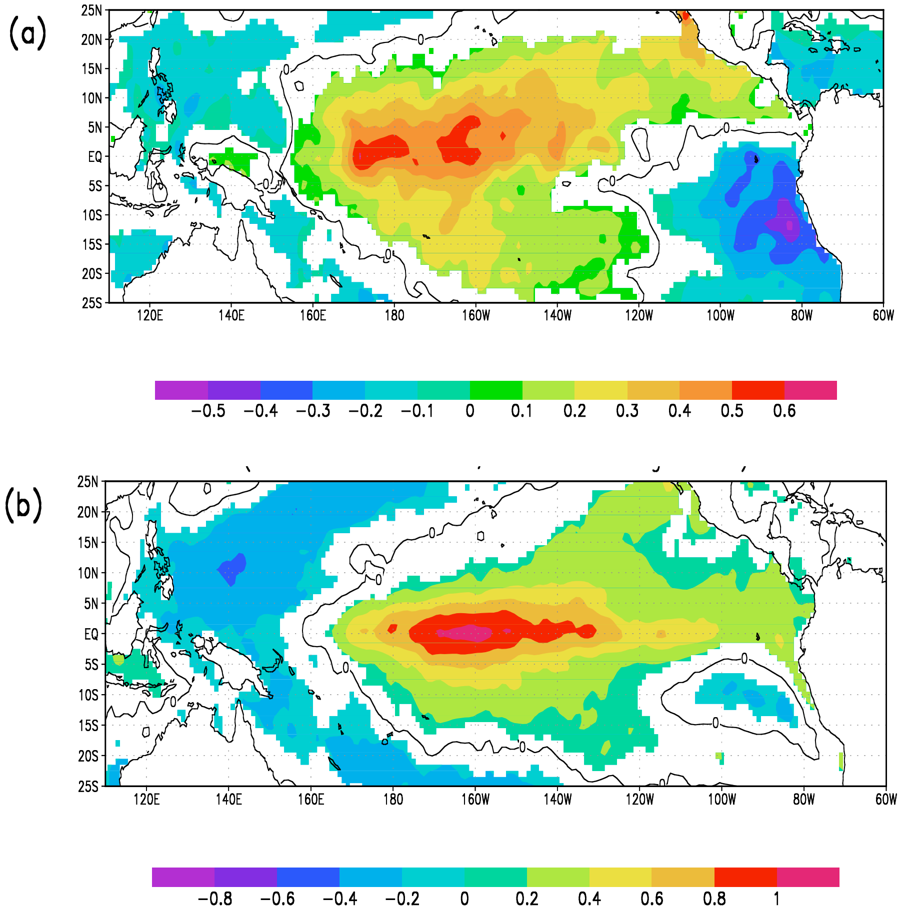

Figure 1: Composite SSTA in ºC during strong positive El Niño Modoki events averaged over (a) seven boreal summers, namely JJAS seasons of 1986,1990, 1991, 1992, 1994, 2002 and 2004 and (b) 8 boreal winters, namely DJF seasons of 1979-80, 1986-87,1990-91, 1991-92, 1992-93, 1994-95, 2002-2003 and 2004-05. Significant values above 95% confidence level from a two tailed Student's t-test are shaded.

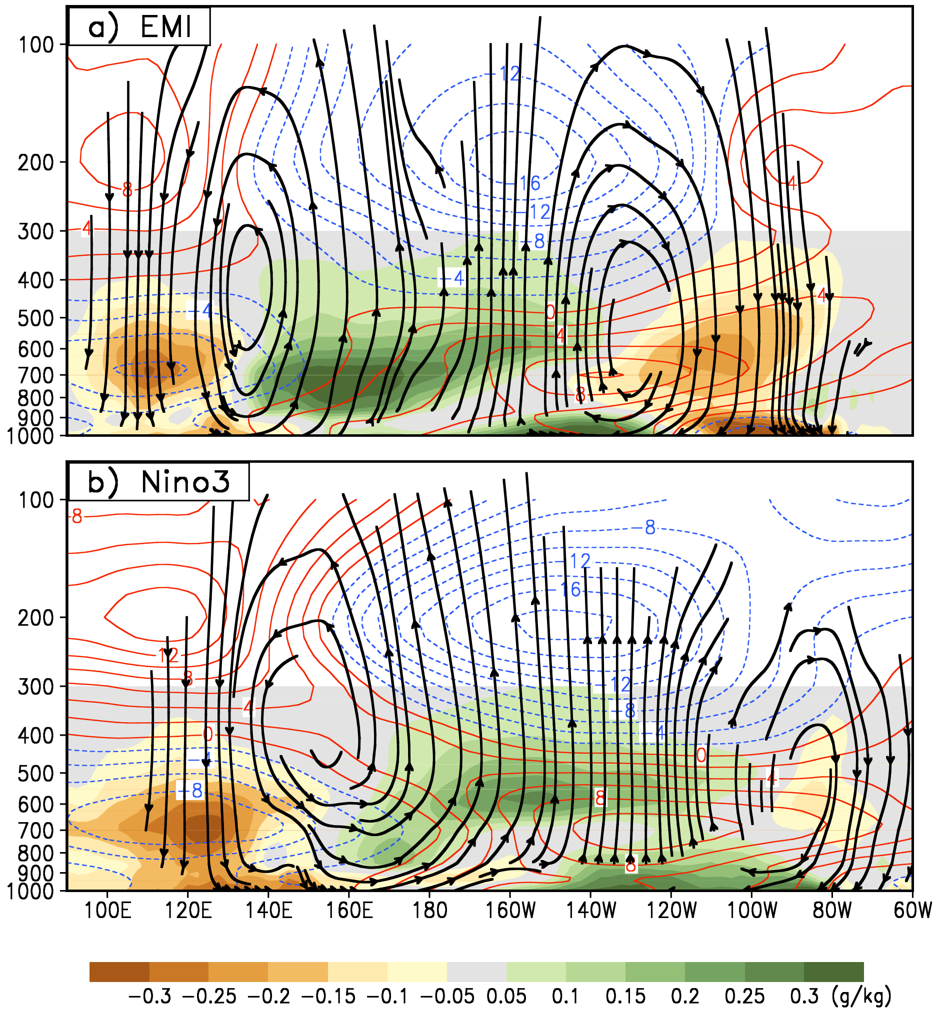

Figure 2: Anomalous Walker Circulations (10S -10N) between 90E and 60W based on partial regression for a) El Niño Modoki Index (EMI) introduced suitably using zonal SST differences and b) Niño3 Index. The vertical velocity at the pressure levels ismultiplied by a factor of -50 to give a better view. The regressed specific humidity is shaded. The contours are for the regressed velocity potential (unit: 10^5 m^2s^{-1}). The units labeled in the regression patterns are actually the units per standard deviation of the index being regressed. The standard deviations for EMI and Niño3 in JJA are 0.504˚C and 0.553˚C, respectively.

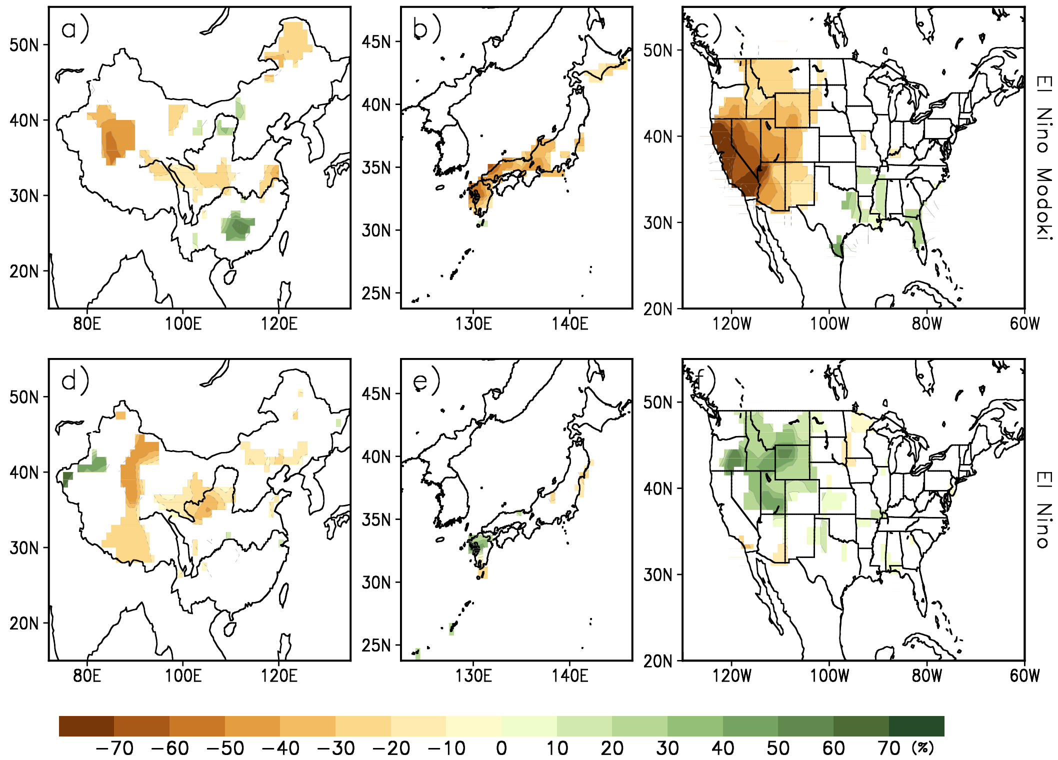

Figure 3: Composite JJA rainfall patterns (anomaly percent of normal: %) for the three largest El Niño Modoki events (1994, 2002, and 2004) in a) China, b) Japan, and c) the United States, and those for the three larges El Niño events (1982, 1987, and 1997) in d) China, e) Japan, and f) the United States. The values with significant levels less than 80% are omitted.

Japanese Initiatives for EU-Japan Collaboration

Hirofumi Sakuma[1]

1: Climate variation research program, FRCGC/JAMSTEC

EU-Japan collaboration on the development of Sintex-F model and climate variability studies started about a decade ago just after the establishment of our research institute Frontier Research Center for Global Change. And the collaboration turned out to be quite fruitful especially with the use of the Earth Simulator (ES) for high-resolution climate simulation done by Sintex-F model. Actually Sintex-F model contributed a lot to the studies on newly discovered Indian Ocean Dipole phenomena especially on identifying its physical mechanism and its influence on the world climate.

We may consider the period over the past 10 years as the first phase of EU-Japan collaboration during which the spirit of the original Sintex project in EU was passed to a new international activity with the powerful research tool of ES. The climate system is a highly nonlinear dynamical system in which the system's behavior crucially depends on the scale interactions extending to a wide range and, in this regard, high resolution simulations attained by ES provide an ample opportunity to investigate the scale interactions important for climate variability. Although climate can be defined as the statistical time mean of daily weather, the resolution of most of the climate simulations so far performed is not fine enough to resolve synoptic scale weather phenomena. The importance of "weather-resolving" climate situation may be appreciated lucidly in the oceanic counterpart of the eddy-resolving simulations ES enabled us to perform them on the global domain. (Fig. 1)

After the success of the basic IOD studies, now the main research activities on Japanese side are gradually shifting from the basic process studies of IOD to the prediction of the short term climate variability. Since the scale interactions in the Indian Ocean region is more active than the Pacific sector, higher resolution simulations done by Sintex-F model are expected to contribute to the basic predictability studies on the short-term climate variability. We believe that one of the main themes of our EU-Japan collaboration in the second phase would be the promotion of the predictability studies along this line of high-resolution simulation experiments. Recently, Asian Pacific Climate Center was established in Korea to share the common goal of our predictability studies and the high-level achievements done or to be done by our EU-Japan collaboration are expected to lead the activities shown in Fig. 2.

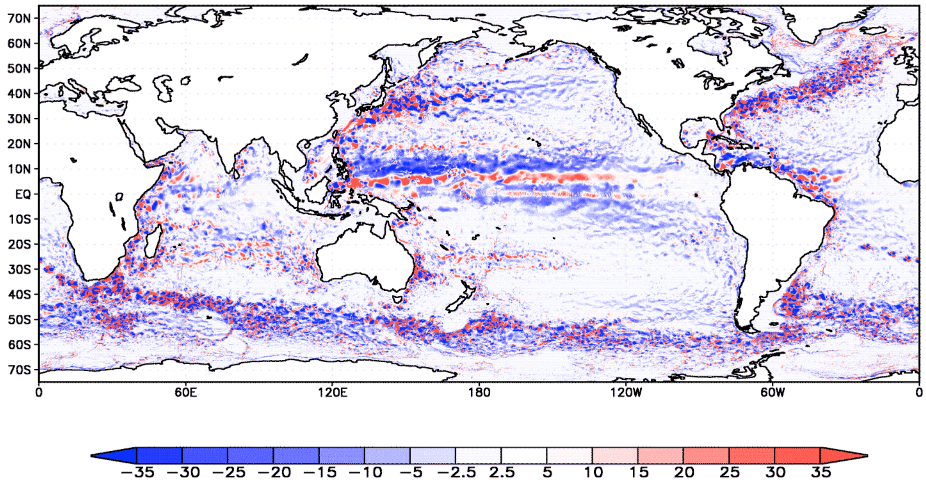

Figure 1: Monthly mean baroclinic activity measured by the potential – kinetic energy conversion rate.

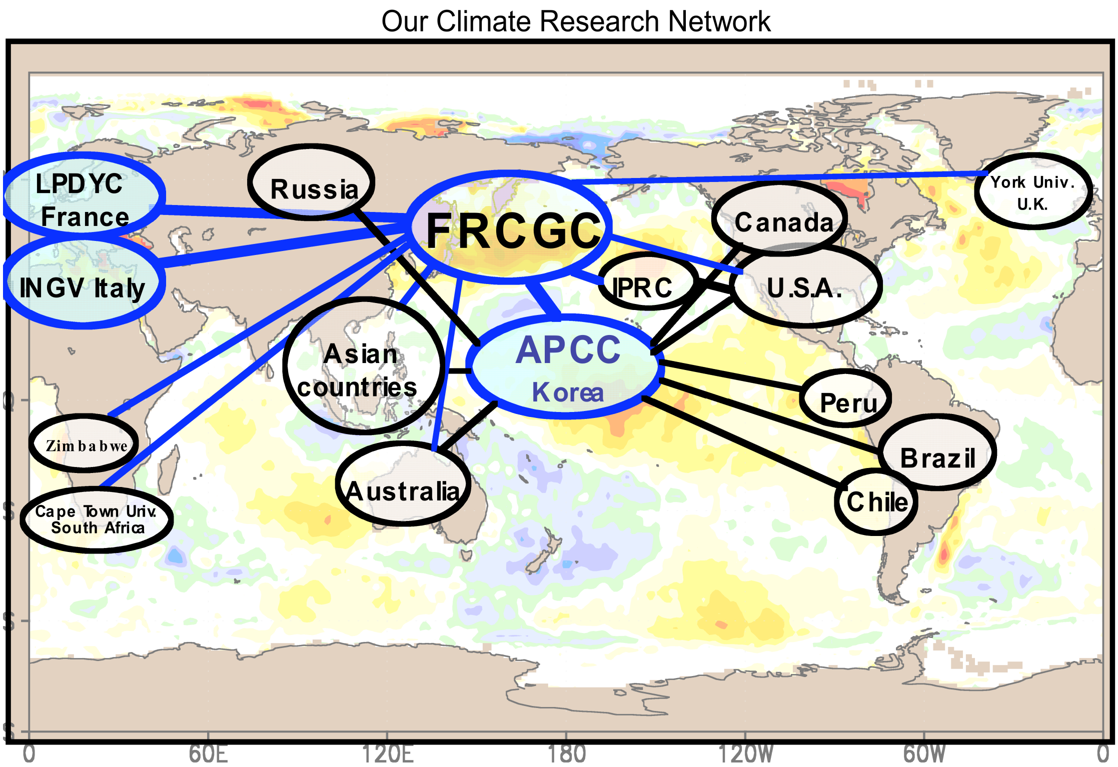

Figure 2: Future network on the climate predictability studies.

Seasonal-to-interannual climate predictability in a fully coupled ocean-atmosphere model

Jing-Jia Luo[1], Sebastien Masson[1], Swadhin Behera[1], and Toshio Yamagata[1]

1: Frontier Research Center for Global Change, JAMSTEC, Yokohama, Japan

Predictabilities of the tropical climate and associated global variations are investigated using a relatively high-resolution SINTEX-F coupled general circulation model. Nine ensemble forecast members are generated by perturbing the model coupling physics which accounts for the uncertainties of both initial conditions and model physics. Owing to the model good performance in simulating the climatology and El Nino-Southern Oscillation (ENSO) in the tropical Pacific, a simple coupled SST-nudging initialization scheme generates realistic thermocline and surface wind variations in the equatorial Pacific. Several westerly and easterly wind bursts in the western Pacific also well captured.

The prediction of ENSO (and its related climate impacts) sufficiently prior to its onset is vital for effective reduction of climate disasters. Retrospective forecasts for the period 1982-2004 show a high predictability of ENSO (Fig. 1). All past El Nino and La Nina events, including the strongest 1997/98 warm episode, are predicted successfully with anomaly skill scores above 0.7 at 12-month lead time. Spatial sea surface temperature (SST) anomalies, teleconnections, and global drought/flood associated with ENSO at its different evolution stages are realistically predicted at 9-12 months lead.

Our extended retrospective forecasts show that several ENSO events over the past two decades can be predicted even at lead times of up to two years. The 1997/98 El Nino event is predicted 21-month ahead despite the influence of active stochastic wind bursts. Two long-lasting La Nina events peaked in 1984-85 and 1999-2000 are predicted well up to 2-year lead. Amazingly, the mild El Nino event of 2002/03 is also predicted well up to 2-year lead, suggesting a link between the prolonged El Nino and the tropical Pacific decadal variability. Seasonal climate anomalies over many regions of the globe during those ENSO years are also realistically predicted up to 2-year lead for the first time.

The Indian Ocean Dipole (IOD), a climate mode similar to ENSO, has also profound socio-economic impacts on various parts of the world as well as countries surrounding the Indian Ocean. Our model is able to predict the extreme positive IOD event in 1994 at 2-3 seasons lead. However, predictability of IOD is limited by the active and chaotic intraseasonal disturbances in the Indian Ocean. Retrospective ensemble forecasts of IOD index for the past two decades showed skillful scores only up to 3-4 months lead and a winter prediction barrier associated with its intrinsic strong seasonal phase-locking. Prediction skills of SST anomalies in both the eastern and western Indian Ocean are higher than those of the IOD index; this is due to influences of the highly predictable ENSO. Encouragingly, increasing ensembles may improve IOD predictions. Our experimental real time forecasts with 18 members successfully predicted the weak negative IOD in 2005 fall and La Nina in 2005/06 winter at two or three seasons lead. The strong positive IOD event in 2006 has been successfully predicted up to one year ahead.

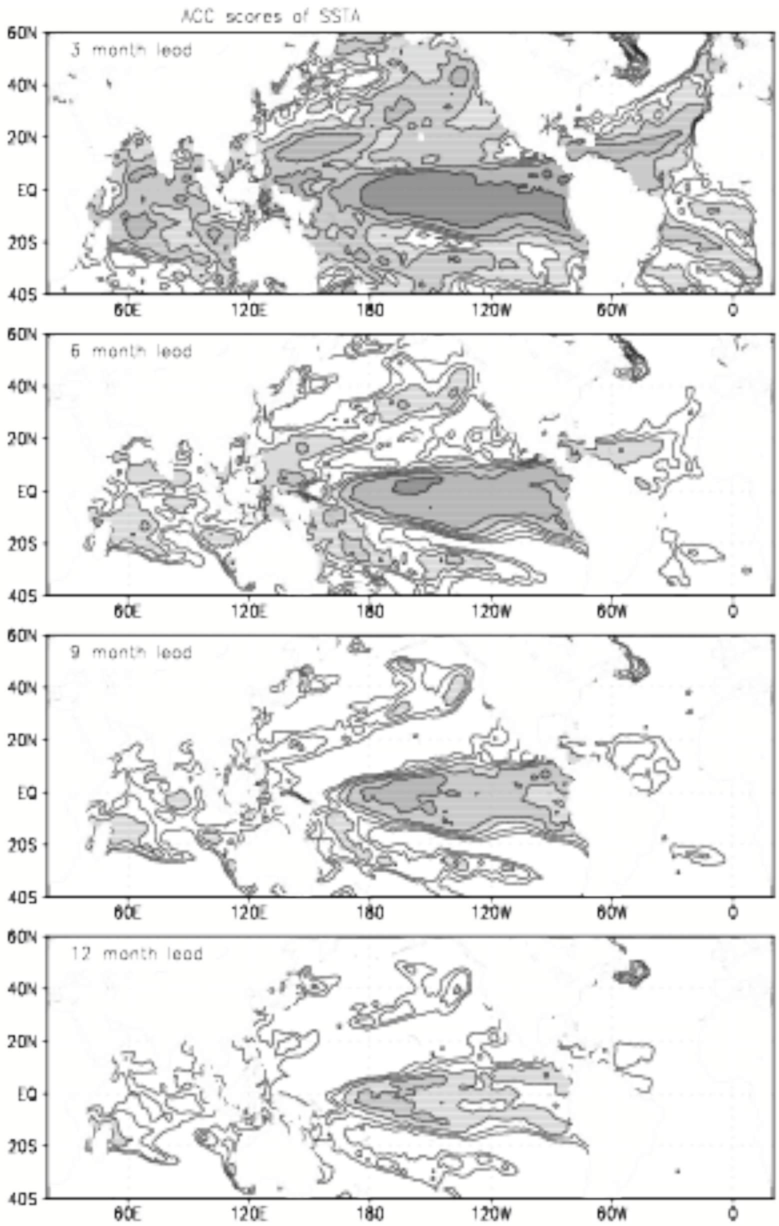

Figura 1: SST anomaly correlations between the NCEP observations and model predictions at different lead times for the period 1982–2004. Contour interval is 0.1 and regions with values above 0.6 are shaded.

Ocean thermodynamics of the simulated ENSO: A seasonally stratified analysis

Tomoki Tozuka[1], Jing-Jia Luo[2], Sebastien Masson[3], and Toshio Yamagata[1,2]

1: Graduate School of Science, The University of Tokyo
2: Frontier Research Center for Global Change/JAMSTEC
3: LODYC

Using outputs from the SINTEX-F1 coupled GCM, thermodynamics of the ENSO events and its decadal modulation are investigated. Simulated El Niño events are first classified into four groups depending on which season the Niño 3.4 SSTA (sea surface temperature anomaly) Index (120°-170°W, 5°S-5°N) reaches its peak. Although the heat content of the tropical Pacific decreases for all four types, it loses about twice as much of heat during El Niño that peaks during winter compared with that peaks during summer.

The surface heat flux, the southward heat transport at 15°S, and the Indonesian Throughflow heat transport contribute constructively to this remarkable seasonal difference. It is shown that differences in the basic state provided by the seasonal cycle cause differences in the atmospheric response to the SSTA associated with the ENSO, which in turn lead to the difference in the surface heat flux and the meridional heat transport anomaly. Since all simulated El Niño events that are followed by another El Niño events peak during boreal spring or summer, and are always characterized by weak or no anomalous heat exports from the tropical Pacific, we suggest that the decadal modulation in the strength of phase-locking to the annual cycle is the key to understand the decadal variation in the characteristics of ENSO.

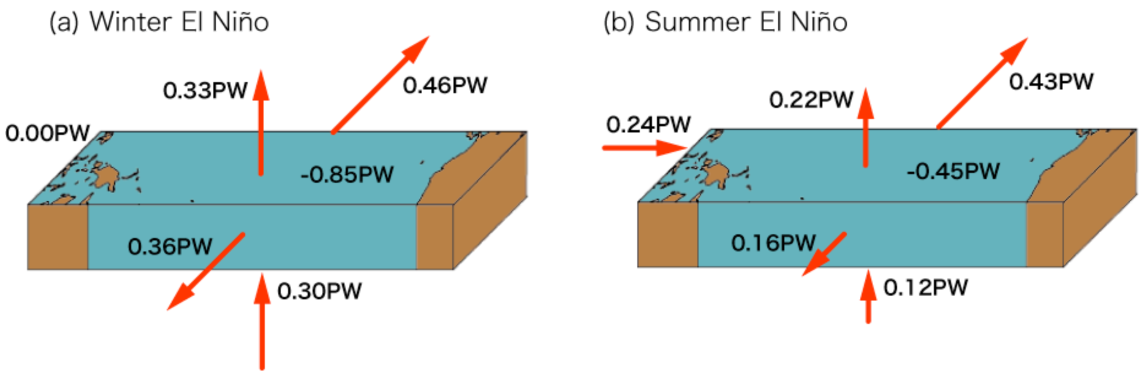

Figure 1: Composite diagrams of heat budget anomaly of tropical Pacific for El Niño events that peak in (a) winter and (b) summer.

Decadal variations of SST in the western North Pacific and associated atmospheric variations in the Sintex-F

M. Nonaka[1], H. Nakamura[1, 2], J.-J. Luo[1], S. Behera[1], H. Sakuma[1], and T. Yamgata[1, 2]

1: Frontier Research Center for Global Change, JAMSTEC
2: University of Tokyo

It has been known that the western North Pacific (NP) region is one of the centers of action of Pacific decadal variability, and several studies have suggested that air-sea interactions in the region may have a key role to induce or intensify the decadal variations. In this study, we examine possible air-sea interaction in the western NP region on the basis of the full coupled integration of the Sinterx-F model.

In the climatological mean, surface heat flux (SHF), precipitation, and pressure fields are represented very well in the Sintex-F model, comparing the reanalysis fields. In the sea surface temperature (SST) field, however, the model has significant warm bias off northern part of Japan due to a northward overshooting of the Kuroshio Current, the western boundary current of the NP subtropical gyre, which is inherent in ocean general circulation models (OGCMs) with non-eddy-resolving horizontal resolution. The western NP region has largest SHF from the ocean to the atmosphere in the Pacific Ocean, and the warm bias in the model induces much stronger upward SHF than in the reanalysis in the region along the northern part of Japan (Figure). With this strong signal of upward SHF, possible ocean-to-atmosphere feedback is apparently found in the model: The strong SHF induces stronger local rainfall and local surface westerly wind with enhanced storm activity and/or vertical mixing, and those reduce vertical wind shear. This property is also hinted in the reanalysis dataset. The enhanced surface wind forms stronger wind-stress curl, which may intensity the subtropical gyre near the western boundary and the northward overshooting of the Kuroshio Current.

In the western NP, more specifically, along the so-called Kuroshio-Oyashio Extension (KOE) front, the zonal oceanic front between the NP subtropical and subarctic gyres, SST has large variance with timescale longer than the El Nino/Southern Oscillation. Lagged correlation analyses on the basis of SST anomalies (SSTAs) in the KOE region show that warm SSTAs in the region are associated with northward migration of the KOE front, and accompanied with upward SHF anomalies, suggesting that the SSTAs are induced by oceanic processes and dumped by the SHF anomalies. The SHF anomalies further enhance local rainfall, surface wind and wind-stress curl fields as found in the climatological fields.

In the NCEP-NCAR reanalysis, similar SSTAs and associated anomalies in the SHF and rainfall are found. The signals, however, are less clear than in the model, and corresponding wind anomalies are not found, suggesting the ocean-to-atmosphere feedback in the model may be slightly too strong. Comparison with a result of an eddy-resolving OGCM suggests that oceanic variations have too direct influence on the SHF field in the Sintex-F model due to its “unified” KOE front, which is also inherent in non-eddy-resolving OGCMs.

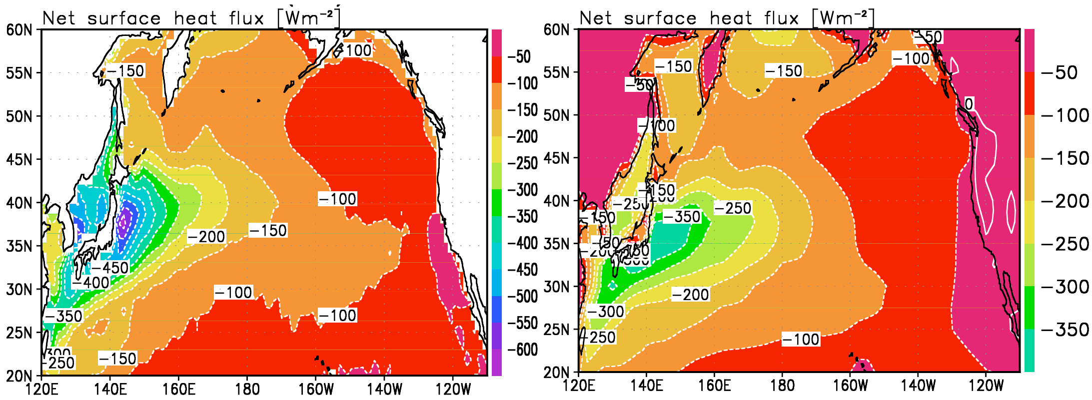

Figure 1: Winter-mean (December-January-February) surface heat flux fields (downward positive) in (left) the Sintex-F full coupled model (Yr 100-150 mean) and (right) ERA40 (1979-2002 mean). Contour intervals are 50 W m^{-2}. Maximum of upward surface heat flux is much larger in the model due to warm SST bias associated with a northward overshooting of the Kuroshio Current.

The Climate Impact of the Intrinsic Indian Ocean Dipole Mode

Swadhin K. Behera, Jing Jia Luo, Sebastien Masson, Suryachandra Rao, Hirofumi Sakuma and Toshio Yamagata

Frontier Research Center for Global Change/JAMSTEC, Showa-machi, Yokohama, Kanagawa 236-0001 Japan

The tropical ocean-atmosphere interactions give rise to coupled climate variations affecting the global climate on several time scales. The El Niño/Southern Oscillation (ENSO) coupled phenomenon of the tropical Pacific was already recognized as one such climate mode. The role of the Indian Ocean coupled mode is realized following the discovery of the Indian Ocean Dipole (IOD) mode (Saji et al. 1999; Yamagata et al. 2004).

The evolution of the IOD is shown to involve active ocean-atmosphere interaction: The coupled mechanism appears to be predominantly dynamical in nature, involving feedbacks between winds and SSTs through upper equatorial ocean dynamics. It is observed that significant IODs evolve in absence of ENSOs though an apparent correlation between the IOD and ENSO, owing to 30% of concurrences, sometime implicate that IOD events are ENSO dependent (e.g. Baquero-Bernal et al 2002). In one of our studies (Behera et al. 2006) we have used SINTEX-F model to study the independent nature of IOD. It is an upgraded version (Luo et al. 2003; Masson et al. 2004) of the SINTEX (Scale INTeraction EXperiment of EU project) model described in Gualdi et al. (2003). In addition to a globally coupled run, a couple of sensitivity experiments are carried out by decoupling the tropical Pacific (non-ENSO) and the tropical Indian Oceans. From the analysis of the non-ENSO experiment results, it is found that the dipole mode takes a dominant seat in SST variabilities of the Indian Ocean instead of the basin-wide monopole mode. The periodicity of interannual IOD is dominantly biennial in non-ENSO experiment results as compared to a quasi-pentadal mode in control experiment results and observation. We find that 58% (82%) of positive IOD events in the control (non-ENSO) experiment evolve from favorable equatorial wind anomalies that are inherent to the Indian Ocean. Cold anomalies from the western tropical Indian Ocean, generated during the boreal fall of the year previous to an IOD, propagate to the Sumatra-Java coast to trigger an IOD event. Based on this early favorable condition, it is deduced that the IOD predictability is higher for independent IOD events as compared to those arising through ENSO influences.

The IOD influences the sea level pressure variability at Darwin, thereby affecting the Southern Oscillation. Through changes in the Walker circulation and water vapor transport, a positive IOD event causes drought in Indonesia and Australia, and flood in eastern Africa. This finding from the observational data of relatively shorter period is well supported by a long record of simulated data derived from the SINTEX-F coupled model. The IOD impact on the East African region overwhelms that of the El Niño/Southern Oscillation (ENSO) during the short rains season that coincides the peak season of IOD (Behera et al. 2005). In fact the present positive IOD event (Fig. 1) in 2006 affected at least 1 million people from the East Africa owing to incessant rainfall (Fig. 2) and associated flooding.

The early signal of the IOD in the SST dipole mode index is shown here to have a very high prediction skill for the variations of short rains. The prediction of extreme years based on the July and August DMI was successful in 92% of cases for the observed data. The August predictability might be higher in case of a longer time series of the data. This is implied from the fact that the successful cases increase up to 94% in case of the SINTEX-F model simulation results. Augmented by the recent advances in the IOD predictability using SINTEX-F (Luo et al. 2007), it is possible to provide reliable information to reduce the disasters and human sufferings from the extremes of short rains.

The IOD influences not only climate fluctuations in the Indian Ocean rim countries but also regions around the globe (Saji and Yamagata 2003). Through atmospheric teleconnection, it is shown that IOD can influence the summer condition over Europe and East Asia including Japan. In the Southern Hemisphere, the IOD related Rossby waves propagate far to the South America to influence the rainfall over La Plata and Brazil during austral spring.

References:

Baquero-Bernal, A., M. Latif, and S. Legutke, 2002: On dipole-like variability in the tropical Indian Ocean. *J. Climate,* **15**, 1358–1368.

Behera, S. K., J.J. Luo, S. Masson, P. Delecluse, S. Gualdi, A. Navarra and T. Yamagata, 2005: Paramount Impact of the Indian Ocean Dipole on the East African Short Rains: A CGCM Study, *J. Climate*, 18, 4514-4530.

Behera, S. K., J.-J. Luo, S. Masson, A. S. Rao, H. Sakuma, and T. Yamagata, 2006: A CGCM Study on the Interaction between IOD and ENSO, *J. Climate,* 19, 1608-1705.

Gualdi S., E. Guilyardi, A. Navarra, S. Masina, and P. Delecluse, 2003: The interannual variability in the tropical Indian Ocean as simulated by a CGCM. *Clim. Dyn.* **20**, 567-582.

Luo, J.J., S. Masson, S. K. Behera, P. Delecluse, S. Gualdi, A. Navarra, and T. Yamagata 2003: South Pacific Origin of the Decadal ENSO-like Variation as Reproduced by a Coupled GCM, *Geophy. Res. Letter*, 30, 2250, doi:10.1029/2003GL018649.

Luo, J.J., S. Masson, S. Behera, and T. Yamagata, 2007: Forecasting the Indian Ocean Dipole using a Coupled OAGCM. *J. Climate,* in press..

Masson, S., J.-J. Luo, G. Madec, J. Vialard, F. Durand, S. Gualdi, E.Guilyardi, S. K. Behera, P. Delecluse, A. Navarra and T. Yamagata, 2004: Impact of barrier layer on winter-spring variability of the southeastern Arabian Sea, *Geophys. Res. Lett.*, 32, L07703, doi:10.1029/2004GL021980.

Rao, S. A., and T. Yamagata, 2004: Abrupt Termination of Indian Ocean Dipole Events in Response to Intra-seasonal Oscillations. *Geophys. Res. Lett.,* **31***, doi:10.1029/2004GL020842.*

Saji, N. H., B. N. Goswami, P. N. Vinayachandran, and T. Yamagata, 1999: A dipole mode in the tropical Indian Ocean. *Nature,* **401**, 360-363.

Saji, N. H., and T. Yamagata, 2003: Possible impacts of Indian Ocean Dipole Mode events on global climate. *Climate Res.*, **25**, 151-169.

Yamagata, T., S. K. Behera, J.-J. Luo, S. Masson, M. Jury, and S. A. Rao 2004: Coupled ocean-atmosphere variability in the tropical Indian Ocean. In *Earth Climate: The Ocean-Atmosphere Interaction*, C. Wang, S.-P. Xie and J.A. Carton (eds.), Geophys. Monogr., **147**, AGU, Washington D.C., 189-212.

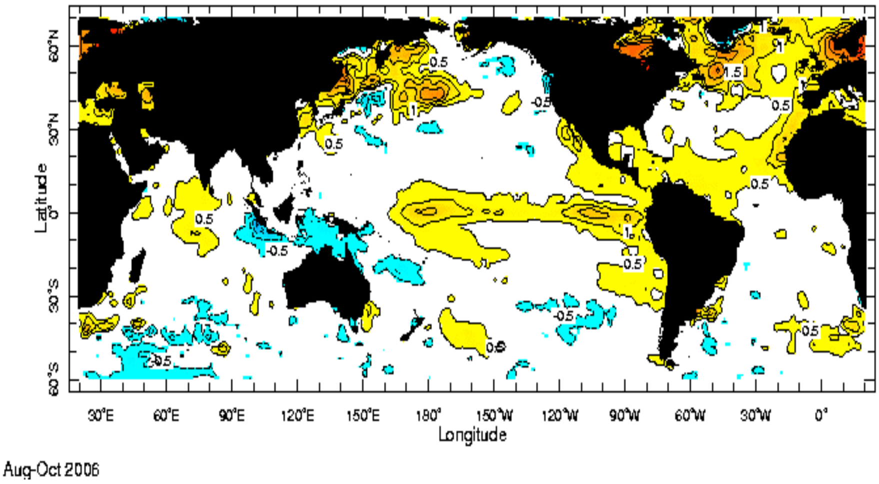

Figure 1: SST anomalies for 2006 August-October season.

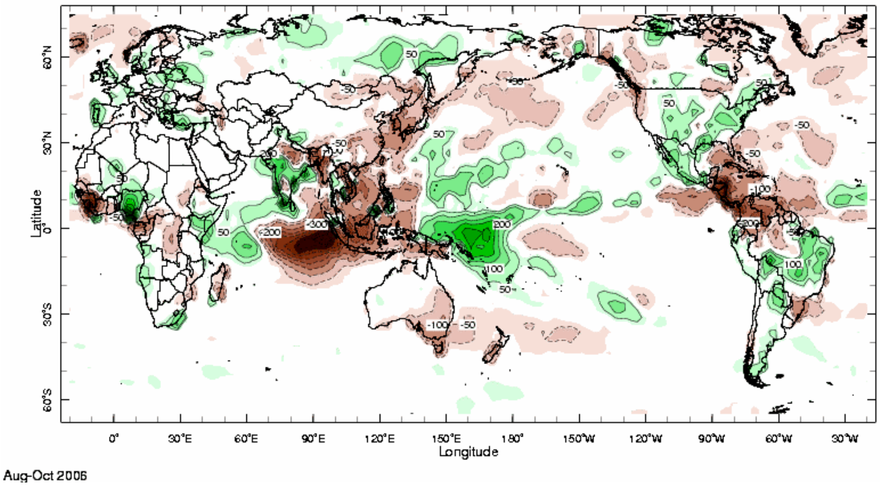

Figure 2: Rainfall anomalies for 2006 August-October season.

ENSO oscillation and the global warming

K. Miyakoda[1], A. Navarra[2], S. Masina[2], A. Cherchi[2], J.J. Ploshay[3]

1: AOS, Princeton University
2: INGV-CMCC Bologna
3: GFDL USA

An analysis is performed on the structure of the ENSO oscillation, using observational data, the atmospheric re-analysis of ECMWF for 44 years (1958-2001) (see Kallberg et al., 2005) and other re-analysis, together with the oceanic data assimilation for 42 years (1958-1999) (see Masina et al., 2001). The conclusions below are mostly based on the results of NDJ (November-December-January) of the La Niña and El Niño years, because the intensities of anomalies are largest in NDJ (or DJF), compared with the intensities for the rest of the years.

One of the main conclusions is that, agreeing with the finding of Hansen et al. (1999), the SST over the El Niño/La Niña region has a sudden change at 1976 from negative to positive anomalies. Some of the reasons will be discussed below. First, the intensity of the " SOI" over the equatorial Pacific has decreased suddenly and substantially. The reason is not subject of this paper. Associated with this change, the rate of the total latent heating has intensified considerably.

The condensation heat, Q_{lat}, emitted during the ENSO period may have contributed not only to sustain but also to increase the atmospheric temperature. This heat is spread from the tropics to the global atmosphere due to the ENSO circulation. In more detail, the condensational heat, Q_{lat}, during the El Niño and La Niña events could be the major sources of the global warming. In particular, this process may have generated the sudden transition of the world SST in 1976. The area of this heat flux is centered around rain belts of the tropics, which extends over the area of 20^0N-20^0S and 80^0E-80^0W.

The ENSO oscillation is the central process for warming/cooling mechanism. It is the atmosphere and ocean coupled system, which contains the condensation of water vapor. The first task in this paper is to construct and draw a reasonable picture of this oscillation. The tropical atmosphere between 30^0N and 30^0S (approximately) and the near-equatorial ocean between 20^0N and 20^0S (approximately) are the main area for the north-south direction, and the tropical Pacific and the Indian Ocean are the east-west extension, with the MC (Maritime Continent) at its center.

Overall El Niños have a characteristic pattern as follows. The atmospheric circulation above 500 hPa level has anti-cyclonic circulations east of the MC for both hemispheres, while it has cyclonic circulation west of the MC. Below 500 hPa level, on the other hand, the circulations described above are all opposite. Concerning the upper ocean, it is characteristic of "a horseshoe pattern" of HC (heat content of the ocean) anomalies in the eastern equatorial Pacific, and "the lobes" in the western off-equatorial Pacific. In the La Niña years, the situation is just opposite to that of the El Niño years. The almost perfect asymmetry of these patterns is observed with respect to the two phases, i.e., La Niña and El Niño. This corresponds to "the tropical biennial oscillation" (see Meehl, 1987).

One of the important evidences in the ENSO process is that the precipitation forms a unique pattern in the near-equatorial area. It is associated with the SPCZ (South Pacific Convergence Zone), the rainy region over the MC, and the ITCZ (Inter-tropical Convergence Zone), and the counter-part over the Indian Ocean, though the patterns are somewhat different depending upon El Niño or La Niña. Compared with the rainfall in non-ENSO periods, the amount of the ENSO precipitation is far greater. In the formation of these rainy belts, the delicate refined structure of ocean current in the near-equatorial zone appears to be important (see Tozuka et al. 2002).

Vecchi and Soden (2007) review a number of atmospheric-oceanic GCMs (general circulation models) submitted to IPCC comparison. According to them, the precipitation patterns and amounts are quite different from each other, indicating that they are most difficult variables to simulate. The reason would be that the precipitation near the equator appears most sensitive to many factors. A view of the present paper is that the vertical velocity in the atmosphere in this region is easily influenced by the upper ocean currents in the area, i.e., the equatorial undercurrent, and the counter current (eastward) at 6^0N, which exists at the depth of 100m for only the Northern Hemisphere. (no counterpart in the Southern Hemisphere).

In order to check the validity of the statements about the importance of latent heat, Q_{lat} in the ENSO region, a number of datasets of rainfall were reviewed following Bosilovich et al. (2007). The datasets are: the ERA-40, the NCEP/NCAR data assimilation, the NCEP-DOE 2nd version, GPCP and the CMAP. Unfortunately, they are very diverse in terms of the time sequence and magnitudes. Among these datasets, the assertion of the present paper agrees well with the result of the ERA-40, secondly with the NCEP 2nd version.

References:

Bosilovich, M.G. et al., 2007: Evaluation of global precipitation in reanalyses. In: *21st Conference on Hydrology at San Antonio, TX.*

Hansen, J. and Coauthors, 1999: GISS analysis of surface temperature. *J. Geophys. Res.*, 104, No. 24, 30,997-31,022.

Kallberg, P. and Coauthors, 2005: Assimilation and modeling of the atmospheric hydrological cycle in the ECMWF forecasting system. *Bull. Amer. Meteor. Soc.*, 86, 387-402.

Masina, S., N. Pinardi, and A. Navarra, 2001: A global ocean temperature and altimeter data assimilation system for studies of climate variabilities. *Clim. Dyn.*, 17, 687-700.

Meehl, G.A., 1987: The annual cycle and interannual variability in the tropical Pacific and Indian Ocean region. *Mon. Wea. Rev.*, 115, 27-50.

Tozuka, T. et al., 2002: Simulated multiscale variations in western tropical Pacific. The Mindanao Dome revisited. *J. Phys. Oceanogr.*, 32, 1338-1359.

Vecchi, G.A. and B.J. Soden, 2007: Global warming and the weakening of the tropical ciculation. To be submitted to J. Climate.

The INGV-CMCC IPCC scenario simulations

E. Scoccimarro[1], S. Gualdi[1,2] and A. Navarra [1,2]

1: Istituto Nazionale di Geofisica e Vulcanologia, Bologna, Italy
2: Centro Euro-Mediterraneo per i Cambiamenti Climatici, Lecce, Italy

This work summarizes the characteristics of the climate simulated by the new global coupled climate model, developed over the last few years at the “Istituto Nazionale di Geofisica e Vulcanologia – Centro Euro-Mediterraneo per i Cambiamenti Climatici” (INGV-CMCC), with the aim of investigating the features and the mechanisms of the climate variability and change during the preindustrial period, the XX century and the scenario simulations performed. The model, named SINTEX-G (SXG), is an evolution of the SINTEX and SINTEX-F models (Gualdi et al., 2003a, 2003b; Guilyardi et al., 2003, Luo et al. 2004). The ocean component is OPA 8.2 (Madec et al., 1998) with the ORCA2 configuration: 2°x2° cos(latitude) with increased meridional resolutions to 0.5° near the equator, 31 vertical levels with 14 lying in the top 150 meters. The atmospheric component is ECHAM4 (Roeckner, 1996) with a T106 horizontal resolution (about 1.125°x1.125°) and 19 hybrid sigma-pressure levels. The coupling information, without flux corrections, is exchanged every two hours by means of the OASIS 2.4 coupler (Valcke et al., 2000).

With respect to the previous version of the model, SINTEX and SINTEX-F, SXG includes a model of the sea-ice (UCL, LIM Louvaine La-Neuve), which allows the production of climate scenario experiments. Here, we present a preliminary analysis of the model results obtained from a simulation of the preindustrial climate, from a 20th Century simulation , from two sres scenarios (A1B and A2) and from two 1%CO_2 increase experiments (to doubling and to quadrupling) (see figure 1).The experiments have been conducted integrating the model with forcing agents, which include greenhouse gases (CO2, CH4, N2O and CFCs) and sulfate aerosols, as specified in the protocol defined for the IPCC simulations (http://www-pcmdi.llnl.gov/ipcc/about_ipcc.php). The annual mean values of the surface temperature field averaged over all latitudes and longitudes, is shown in Figure 2 for the model simulations and observations. The curves represent the deviation of the annual mean surface temperature with respect to the 1870-1900 mean. The observations (black curve) show the well known global warming trend of about 0.6°C over the past century. The model simulation (brown curve) exhibits a similar trend, though slightly more pronounced, over the same period.

At the end of the sres A1B and A2 simulation, the model reach respectively a global warming trend of about 3.2 ^{o}C and 4 ^{o}C.

The major difference between SXG and the previous versions of the model (SINTEX and SINTEX-F) is the inclusion of a thermodynamic-dynamic model that describes the evolution of the sea-ice. Therefore it is of interest to assess, at least in a qualitative sense, the ability of the model to reproduce the gross features of the observed sea-ice.

To this aim, Figures 3 and Figure 4 show the climatological observed and simulated sea-ice distribution for both winter and summer seasons in the northern hemisphere and southern hemisphere respectively. The observations (Figure 3 and Figure 4, panels c and d) are from the NASA NSIDC (National Snow and Ice Data Center) DAAC (Distributive Active Archive Center). The results indicate that the model captures reasonably well the basic seasonal features of the sea-ice distribution both in the Northern and in the Southern Hemisphere, even if it appears to underestimate the sea-ice concentration during the winter season.

In order to explain the behavior of the model in represent the Sea-Ice dynamics, we calculate the volume of the Sea-Ice stored in the two hemispheres: At the end of the XX century simulastion, in the northern emisphere, the Sea-Ice volume is reduced to 40% with respect to the beginning of the century; in the southern emisphere the melting effect is less pronunced: the Sea-Ice volume is reduced to 65%. In the sres A1B and A2 simulations, the more pronunuced melting effect in the northern emisphere is maintained.

References:

Gualdi, S., A. Navarra, E. Guilyardi, and P. Delecluse, 2003a: Assessment of the tropical Indo-Pacific climate in the SINTEX CGCM, Ann. Geophysics, 46, 1-26.

Gualdi, S., E. Guilyardi, A. Navarra, S. Masina, and P. Delecluse, 2003b: The interannual variability in the tropical Indian Ocean as simulated by a CGCM. Clim. Dyn., 20, 567-582.

Guilyardi, E., P. Delecluse, S. Gualdi, and A. Navarra, 2003: Mechanisms for ENSO phase change in a coupled GCM, J. of Clim., 16, 1141-1158.

Luo, J.-J., S. Masson, S. Behera, P. Delecluse, S. Gualdi, A. Navarra, and T. Yamagata, 2003: South Pacific origin of the decadal ENSO-like variation as simulated by a coupled GCM. Geophys. Res. Lett., 30, 2250, doi:10.1029/2003GL018649.

Madec, G., P. Delecluse, M. Imbard, and C. Levy, 1998: OPA 8.1 Ocean General Circulation Model reference manual, Internal Rep. 11, Inst. Pierre--Simon Laplace, Paris, France.

Roeckner E, and Coauthors, 1996. The atmospheric general circulation model Echam-4: model description and simulation of present-day climate. Max-Planck-Institut fur Meteorologie, Rep. No 218, Hamburg, Germany, 90 pp.

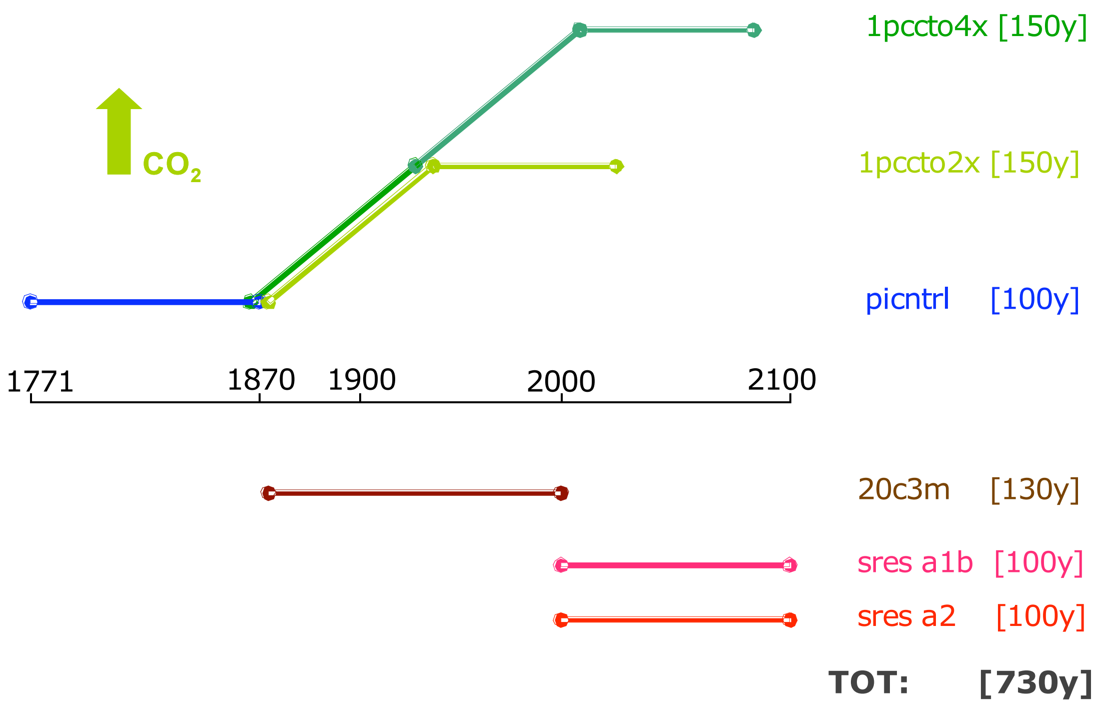

Figure 1: IPCC climate simulations performed at INGV-CMCC.

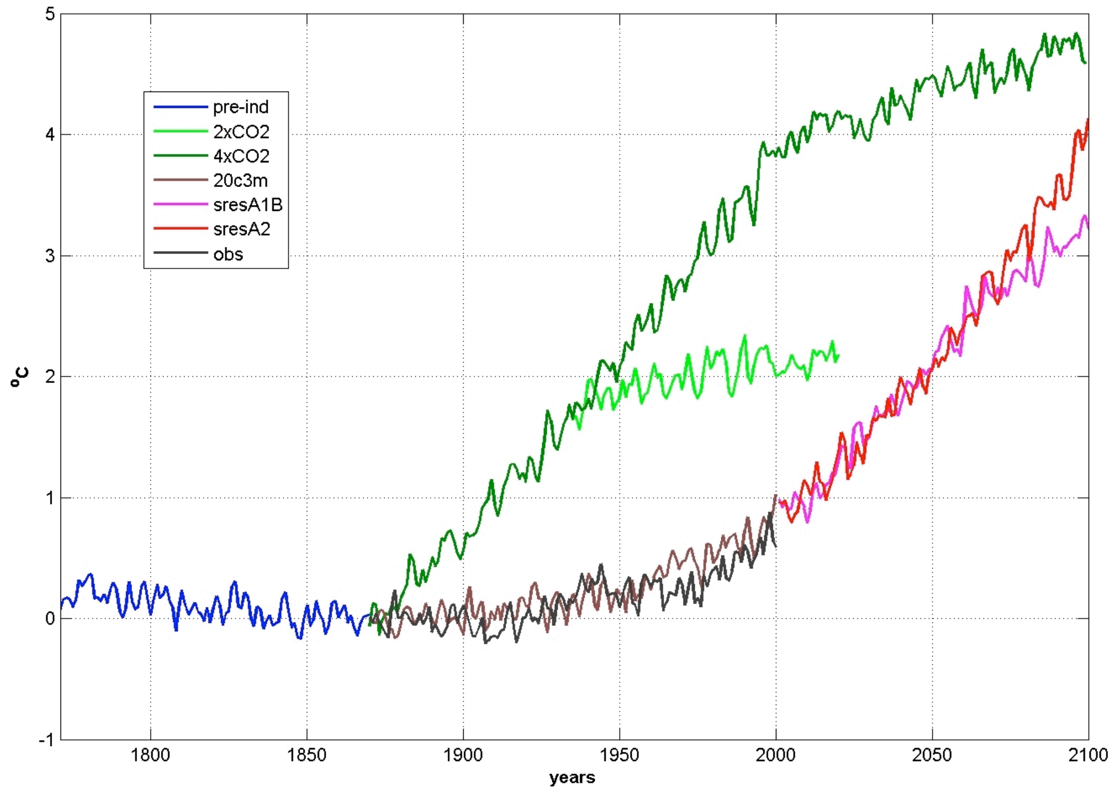

Figure 2: global temperature anomaly in INGV-CMCC IPCC simulations with respect to the period 1870-1900.

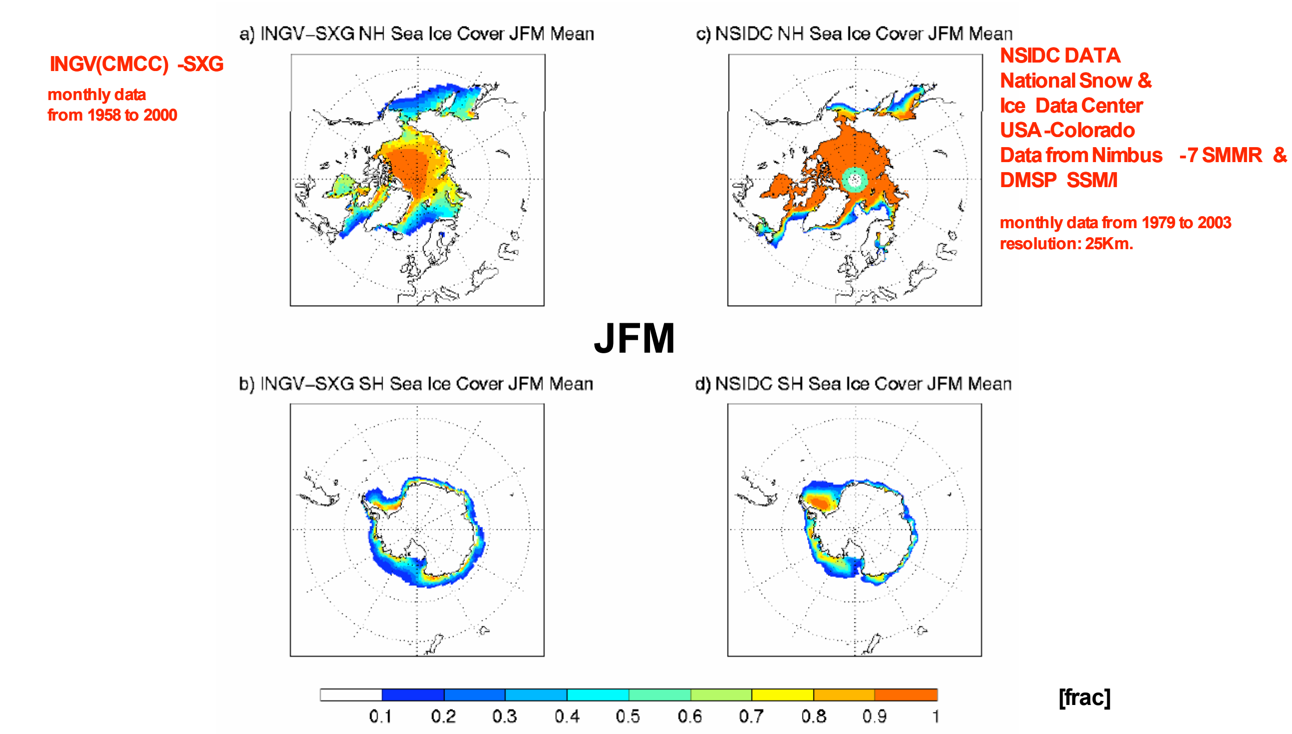

Figure 3: Sea-Ice distribution northern winter season.

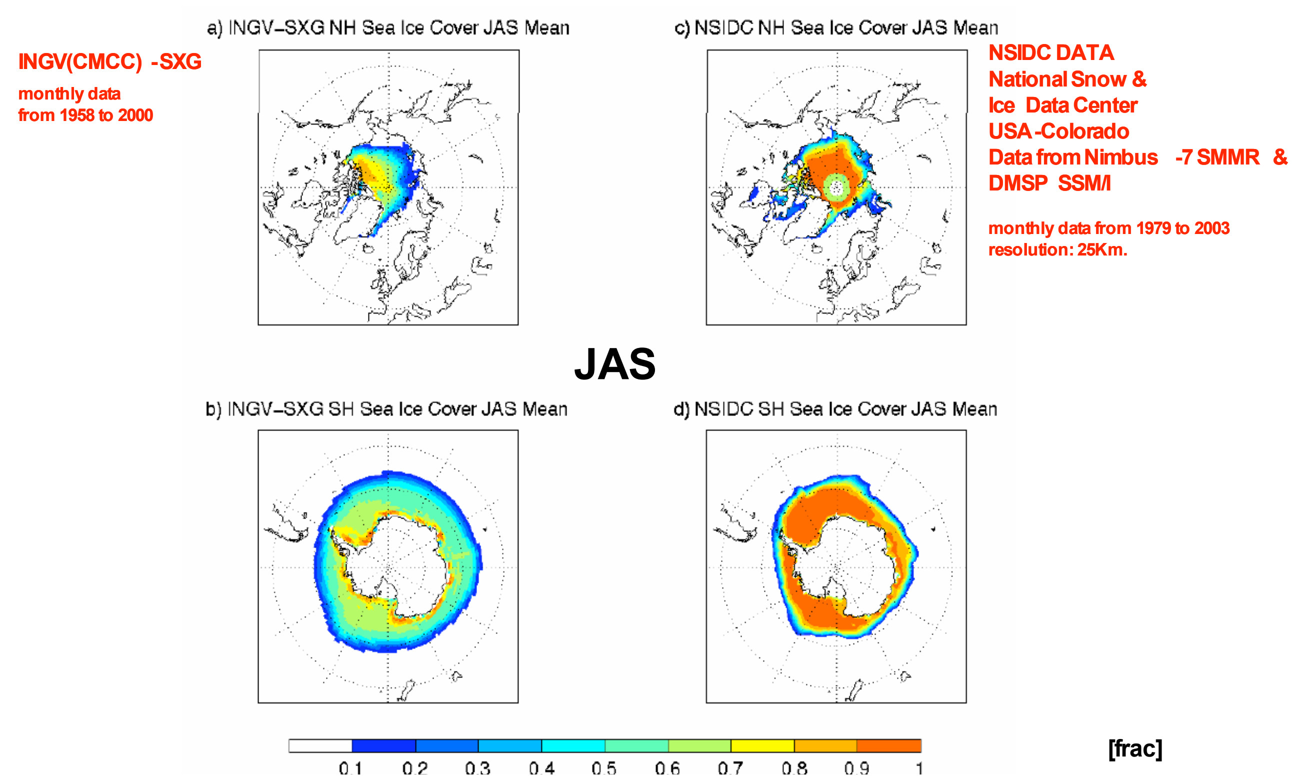

Figure 4: Sea-Ice distribution northern summer season.

INGV(CMCC) IPCC Scenario Simulations: Changes in the Tropical Climate

S. Gualdi[1,2], E. Scoccimarro[1], and A. Navarra [1,2]

1: Istituto Nazionale di Geofisica e Vulcanologia, Bologna, Italy
2: Centro Euro-Mediterraneo per i Cambiamenti Climatici, Lecce, Italy

This study investigates the possible changes that the greenhouse global warming might generate in the characteristics of the tropical cyclones (TCs). The analysis has been performed using scenario climate simulations carried out with a fully coupled high–resolution (T106) global general circulation model.

The capability of the model to reproduce a reasonably realistic TC climatology has been assessed by comparing the model results from a simulation of the 20th Century with observations. The model appears to be able to simulate tropical cyclone-like vortices with many features similar to the observed TCs. The simulated TC activity exhibits realistic geographical distribution (Figure 1). Also the observed pronounced seasonal modulation of the TC activity (not shown) is correctly captured. Furthermore, the model appears to produce a realistic interannual variability of the number of TCs in most of the tropical regions , with a correlation between TC occurrence and ENSO episodes which is fully consistent with the observations.

All these results suggest that the model is able to reproduce the major basic mechanisms that link the TC occurrence with the large scale circulation and that it represents a suitable tool for assessing the possible changes that TC climatology can undergo as a consequence of the greenhouse global warming.

The results from the climate scenarios reveal a substantial general reduction of the TC frequency when the atmospheric $CO2$ concentration is doubled and quadrupled (Figure 2). The reduction appears particularly evident for the tropical north west Pacific (NWP) and north Atlantic (ATL). In the NWP the weaker TC activity seems to be associated with a reduced amount of convective instabilities due to a rise of the level of free convection.

In the ATL region the weaker TC activity seems to be due to both the increased stability of the atmosphere (Figure 3) and a stronger vertical wind shear (not shown). Despite the generally reduced TC activity, there is evidence of increased rainfall associated with the simulated cyclones. Despite the overall warming of the tropical upper ocean and the expansion of warm SSTs to the subtropics and mid-latitudes, the action of the TCs remains well confined to the tropical region and the peak of TC number remains equatorward of 20◦ latitude in both Hemispheres.

Our findings are in full agreement with the results obtained in similar studies but with atmospheric only models (e.g Yoshimura et al. 2006). For a more complete discussion of our results and an extended comparison with other studies the reader is addressed to Gualdi et al. (2007).

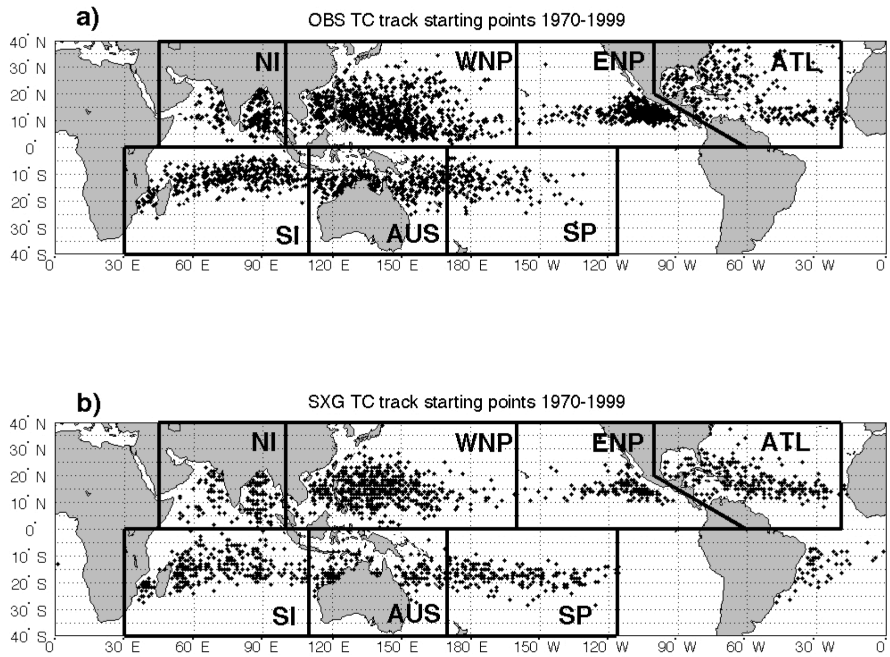

Figure 1: Distribution of the TC track starting points for the period 1970-1999 for the observations (panel a) and model (panel b). Each point corresponds to the geographical location of a TC at the time of its first detection. Following Camargo et al. (2004) seven regions of TC genesis have been defined. In the pictures these regions are delimited by thick black lines.

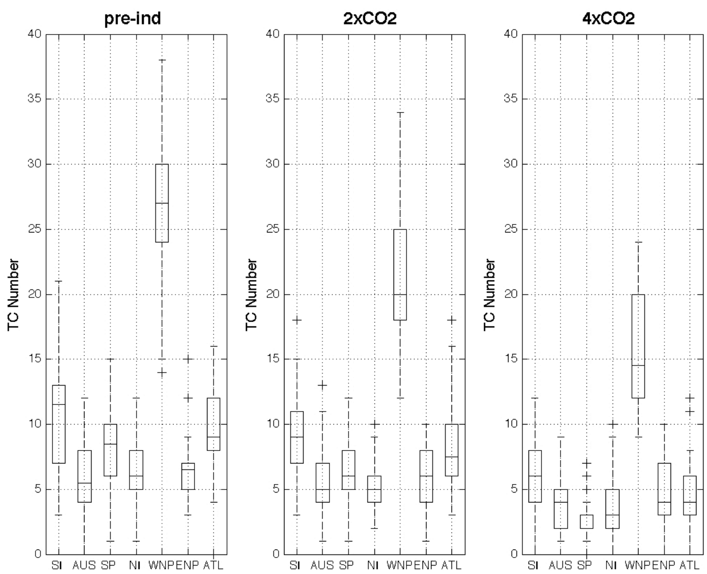

Figure 2: Box plot of the annual number of TCs in the areas defined in Figure 1 and for the PREIND experiment (left panel), 2CO2 experiment (middle) and 4CO2 experiment (right panel).

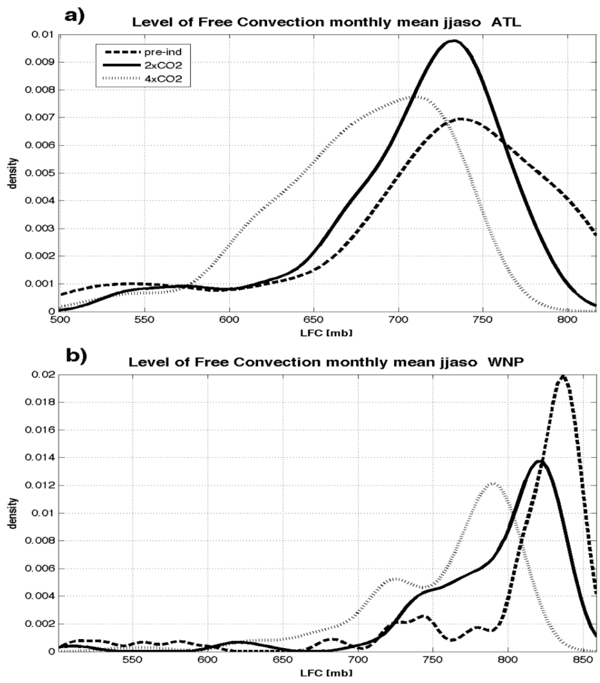

Figure 3: Probability distribution function (PDF) of the level of free convection (LFC) for the PREIND case (dashed), the 2CO2 case (solid line) and the 4CO2 experiment (dotted curve) over the ATL region (panel a) and the WNP region (panel b) during northern summer (JJASO). On the x-axis is the value of vertical levels in Millibar (mb), and on the y-axis is the (density of) frequency of occurrence at which free convection can be triggered at that level. The pictures show a rise of the LFC to higher levels when the atmospheric CO2 is increased. Higher LFCs imply less convective activity.

References:

Gualdi S., E. Scoccimarro, and A. Navarra, 2007: Changes in Tropical Cyclone Activity due to Global Warming: Results from a High-Resolution Coupled General Circulation Model. J. of Clim., submitted.

Yoshimura J., M. Sigu, and A. Noda, 2006: Influence of greenhouse warming on tropical cyclone frequency. J. Meteor. Soc. Japan, 84, 405–428.

Multiannual variability in the North Atlantic climate system: NAO/Ocean circulation interactions in the INGV/CMCC coupled GCM.

Alessio Bellucci[2], Silvio Gualdi[1,2], Enrico Scoccimarro[1] and Antonio Navarra[1,2].

1: Istituto Nazionale di Geofisica e Vulcanologia, Bologna, Italy
2: Centro Euro-Mediterraneo per i Cambiamenti Climatici, Lecce, Italy

Introduction

The NAO is the leading variability mode of the North Atlantic sector, characterised by a redistribution of atmospheric mass between the Arctic and the subtropical Atlantic. The NAO is particularly prominent during the boreal winter, and explains more than 36% of SLP variance in JFM (Hurrell et al., 2003). The NAO pattern displays temporal variability (generally measured as the normalized pressure gradient between Iceland and Azores – the so called NAO index (NAOI)) over a broad spectrum of timescales, ranging from interannual to decadal and longer. The dynamics underlying the low frequency tail of the NAOI are not well understood. A particularly crucial aspect of decadal variability in the NAO is the role played by the ocean. Is the ocean simply passively driven by the atmosphere, or does the coupling with the overlying atmosphere determine enhanced spectral power over decadal timescales? According to the climate noise paradigm (Madden, 1981) the low frequency NAO variability is determined by processes which are intrinsic to the atmosphere.

Marshall et al. (2001) , Czaja and Marshall (2001) and D'Andrea et al. (2005), using idealized configurations of the coupled ocean-atmosphere system, suggest that ocean dynamics introduce a significant departure from the climate noise paradigm, with the ocean circulation determining the onset of a damped oscillatory mode in the North Atlantic sector involving coordinated changes in the SST and atmospheric circulation, with a typical NAO-like structure (a mechanism which is generally referred to as the *delayed oscillator* paradigm).

In the present study, the interplay between mid-to-high latitude SST, ocean circulation variability and the NAO is analysed in detail, with a full-fledged coupled general circulation model (CGCM). A major focus of this study is the role of ocean circulation on the NAO variability, with specific attention to the barotropic wind-driven component. In particular, the role of the Inter-Gyre Gyre (IGG; Marshall et al. 2001) as a heat carrier, and its impact on the low frequency modulation of the North Atlantic SST tripole is investigated. A mechanism governing the oscillation is identified, bearing strong similarities with the *delayed oscillator* paradigm (Marshall et al. 2001).

Model:

Results from the 20C3M IPCC experiment performed with the INGV/CMCC coupled general circulation model (Gualdi et al. 2006) are analysed. We focus on the boreal winter period (JFM), when the NAO signature is particularly intense.

The SST tripole:

First we analyze the temporal and spatial structure of the JFM SST variability in the North Atlantic sector. The leading EOF of boreal winter SST displays the well known tripole pattern, with anomalously cold SST over the subpolar basin, a warm subtropical centre of action and a cold lobe in the tropics.

We use the associated principal component (PC1) as an index of the temporal variability of the tripole. In order to inspect the space structure associated with the leading temporal scales of the tripole variability we perform a composite analysis based on the PC1, at different time-lags.

After selecting the years for which the PC1 in absolute value exceeds one standard deviation, we average the SST anomalies over the years with a high tripole index and subtract the average computed over low index years. The resulting composite map provides the lag-0 SST anomalies, reproducing the previously described tripole pattern. The composite map for the following 1 year-lag is obtained by subtracting the low index +1 year average from the high index +1 year average.

The same procedure is applied for several temporal lags. The sequence of lagged composite maps (shown in figure 1) reveals that the tripole structure disapperars after 1 year, but re-emerges 5 years later, with a reduced amplitude. Since the thermal intertia of the mixed layer accounts for an ocean memory of a few months (according to Frankignoul et al. 1998), the reappearance of the tripole a few years later suggests that an additional process sustaining the leading SST variability pattern must be at work.

The coherency between SST variability and NAOI is now analyzed by means of point-wise correlations between the NAOI and SST at different time-lags (not shown). At lag-0, a tripole pattern is recovered, indicating an instantaneous local response of the upper ocean to the positive phase of the NAO (NAO+), through turbulent heat fluxes. At the following lags, a propagating structure can be identified, approximately following the NAC pathway, reaching the Labrador Basin in a 2-3 years time, after an NAO+ event, thus determining an inversion in the sign of the northern dipole. In figure 2, regions where correlation exceeds 0.2 are shown, for lags 0 to +3 years (significant at the 95% level). The poleward propagation indicates that changes in the Labrador Basin SST are coherent with an NAO+ event which occurred three years before.

An Hovmoller diagram of SST anomalies along the track of the mean propagation pathway which can be identified from the lagged-correlation maps, reveals the existence of drifting SST anomalies, consistent with the propagating structures detected in the NAOI/SST correlation patterns (not shown). The thermal anomalies mean propagation velocity is approximately equal to 6 cm/s.

The role of ocean circulation:

The role of ocean circulation in the poleward propagation of thermal anomalies is now investigated.

First we relate changes in the NAO with basin-wide changes in the ocean circulation. We ideally split the large-scale ocean transport into a horizontal barotropic (mainly wind-driven) component, and a (mainly buoyancy-driven) meridional overturning circulation.

Barotropic circulation:

The dominant variability pattern associated with the barotropic streamfunction (figure 3, right panel) displays an anti-cyclonic anomaly having an approximate 5 Sv strength (1 Sv=10^6 m^3/s), which is slightly shifted to the north with respect to the mean subtropical gyre (now shown), and a weaker cyclonic circulation anomaly in the western subpolar basin, which locally intensifies the mean cyclonic circulation in that area. The anomalous anti-cyclonic gyre - generally referred to as Inter-Gyre Gyre (IGG;Marshall et al. 2001) – and the subpolar cyclonic circulation anomaly, appear to be consistent with the NAO wind-curl pattern (figure 3, left panel). The JFM composite of wind-stress keyed to the NAOI at lag 0, for index values exceeding 1 standard deviation, shows a predominantly anticyclonic anomaly over the subtropics, and a cyclonic vorticity anomaly over the subpolar region. Thus the leading variability mode of the barotropic circulation appears to be consistent with a Sverdrup-type response to the NAO wind-stress, with the NAO-wind torque balanced by meridional advection of planetary vorticity:

$$\Psi(x,\phi) = -\frac{a\tan\phi}{\rho_0}\int_{x_E}^{x}\mathbf{k}\cdot(\nabla\times\frac{\tau}{f})dx'$$

The coherency between the horizontal circulation and the NAO is analysed by means of lag-correlation maps between of barotropic streamfunction against the NAOI (not shown). The largest correlations are found at lag 0 and +1 year, nearby the cross-gyre subtropical/subpolar boundary.

The immediate (lag 0) response to a NAO+ event is an intensified inter-gyre transport. For later time-lags, the positive correlation structure which characterizes the subtropics, propagates to the west. At lag +4, the sign of the northern "correlation dipole" has reversed, with respect to the fast lag-0 response, indicating a weakening of the mean gyre circulation, close to the cross-gyre boundary (although the subpolar positive correlation is not statistically significant for that lag).

Meridional overturning circulation:

We now analyse the relationships between the NAOI and basin-wide changes in the meridional overturning circulation through point-wise correlation maps of the meridional overturning streamfunction against the NAOI for several lags. At lag 0, the fast Ekman transport response to the NAO windstress signature drives two shallow circulation cells in the upper 100 meters. A stronger correlation, emerges at lag +1 year, with a dipole centered around 40N, implying an intensification of the mean meridional overturning cell at northern latitudes, and a weakening of the overturning south of 40N. The positive correlation structure propagates southward at successive lags (while the negative pole decays) until the dipole reappears with reversed sign at lag +4. The lagged response of the meridional overturning circulation has a column-wise structure, suggesting that during an NAO+ phase increased westerlies over the subpolar region induce – through local turbulent heat fluxes - anomalously high buoyancy losses leading to the onset of deep convection.

Meridional Heat Transport:

In order to evaluate the relative impact of gyre and overturning circulation on the poleward heat transport, we compute the lagged correlation of NAOI against meridional heat transport at the cross-gyre boundary (around 51N; figure 4). The lagged correlation is asymmetric with respect to zero lag, indicating a delayed response of the large-scale circulation to the NAO, for both the barotropic and meridional overturning circulation, reaching a maximum positive correlation after 1 and 2 years respectively. The correlation is found to be larger for the horizontal gyre contribution, which closely follows the total meridional heat transport. Significant correlations (at the 95% level) are found for the gyre component only (so we will neglect the overturning component in the following discussion).

The lagged correlation does also reveal a 5 years characteristic time-scale, suggesting that the system undergoes a damped sub-decadal oscillation. A possible mechanism underlying such oscillatory mode is sketched below.

The positive correlation at lag +1 indicates that NAO+ drives (through an enhanced IGG strength) a delayed poleward heat transport which concurs to a warming of the subpolar gyre. A warming in the subpolar region decreases the meridional SST gradient (hence weakening the SST tripole) which sets favourable conditions for the NAO to enter into a negative phase (NAO-). This in turn produces a weaker northward heat transport, restoring cooler conditions at the northern latitudes.

Conclusions:

We provide evidence of a damped oscillatory mode of the North Altantic sector in a state-of-the-art CGCM having a typical sub-decadal time-scale. The oscillation involves the interplay between NAO-related changes to the wind stress curl, the barotropic ocean circulation, and the propagation of SST anomalies. In particular, the anomalous wind-driven circulation associated with the NAO wind-torque is responsible for carrying heat through the subtropical/subpolar gyre boundary, which in turn modulates the northern lobe of the SST tripole. The low frequency modulation of the SST tripole in turn sets the condition for changes of the NAO phase itself.

These results appear to be qualitatively consistent with similar results obtained in either theoretical, or highly simplified GCMs. In particular, there is consistency with the *delayed oscillator* theoretical model (Marshall et al. 2001; M01) but the time scale of the IGG spin-up is faster than predicted by M01.

This might be due to the strong damping of high-order baroclinic Rossby waves in a highly dissipative low resolution OGCM, determining a rapid adjustment of the barotropic circulation to changes in the wind-stress curl.

References:

Czaja A. and J. Marshall, 2001: Observations of atmosphere ocean coupling in the North Atlantic,*Quart. J. Roy. Meteor. Soc.*, **127**, 1893-1916.

D'Andrea F., A. Czaja and J. Marshall, 2005: Impact of anomalous ocean heat transport on the North Atlantic Oscillation, *J. Climate*, **18**, 4955-4969.

Frankignoul, C., A. Czaja and B. L'Heveder, 1998: Air-sea feedback in the North Atlantic and surface boundary conditions for ocean models, *J. Climate*, **11**, 2310-2324.

Hurrell, J. W., G. Ottersen, Y. Kushnir and M. Visbeck, 2003: An overview of the North Atlantic Oscillation, in *The North Atlantic Oscillation: climatic significance and environmental impact*, edited by J. Hurrell, Y. Kushnir, G. Ottersen, and M. Visbeck, American Geophysical Union, Geophysical Monograph 134.

Madden, R. A., 1981: A quantitative approach to long-range prediction, *J. Geophys. Res.*, **86**, 9817-9825, 1981.

Marshall, J., H. Johnson and J. Goodman, 2001: A study of the interaction of the North Atlantic Oscillation with ocean circulation, *J. Climate*, **14**, 1399-1421.

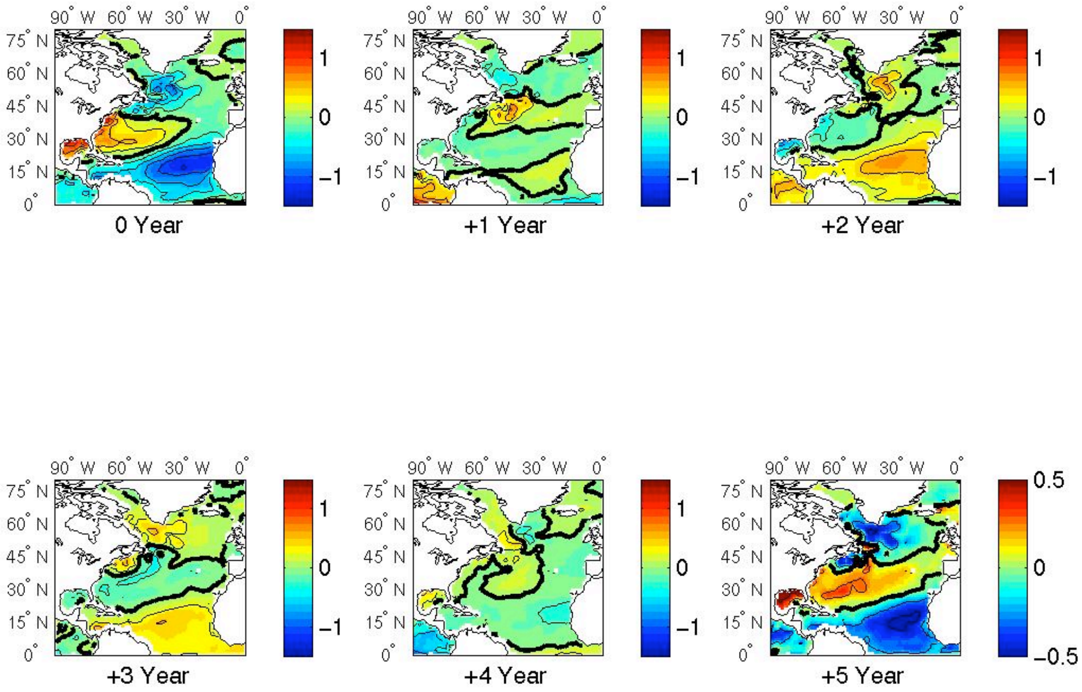

Figure 1: Composite of winter SST anomalies based on years where the SST PC1 is higher (in absolute value) than 1 standard deviation (see text for details). SST anomalies are contoured every 0.25K. The black thick line indicates the 0K isoline.

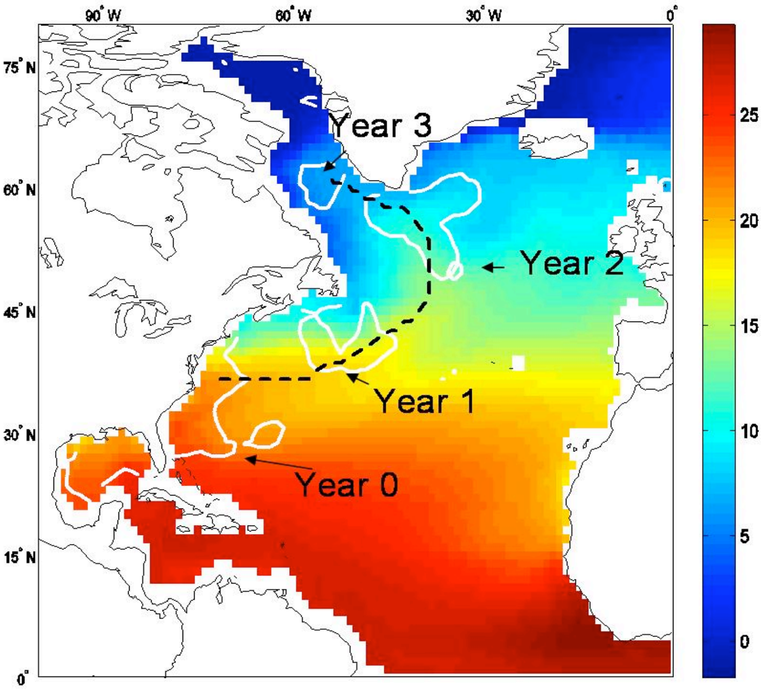

Figure 2: White contours indicate areas where the NAOI vs SST correlations exceed 0.2 (significant at the 95% confidence level) for several time-lags. The mean SST is also shown (color shading).

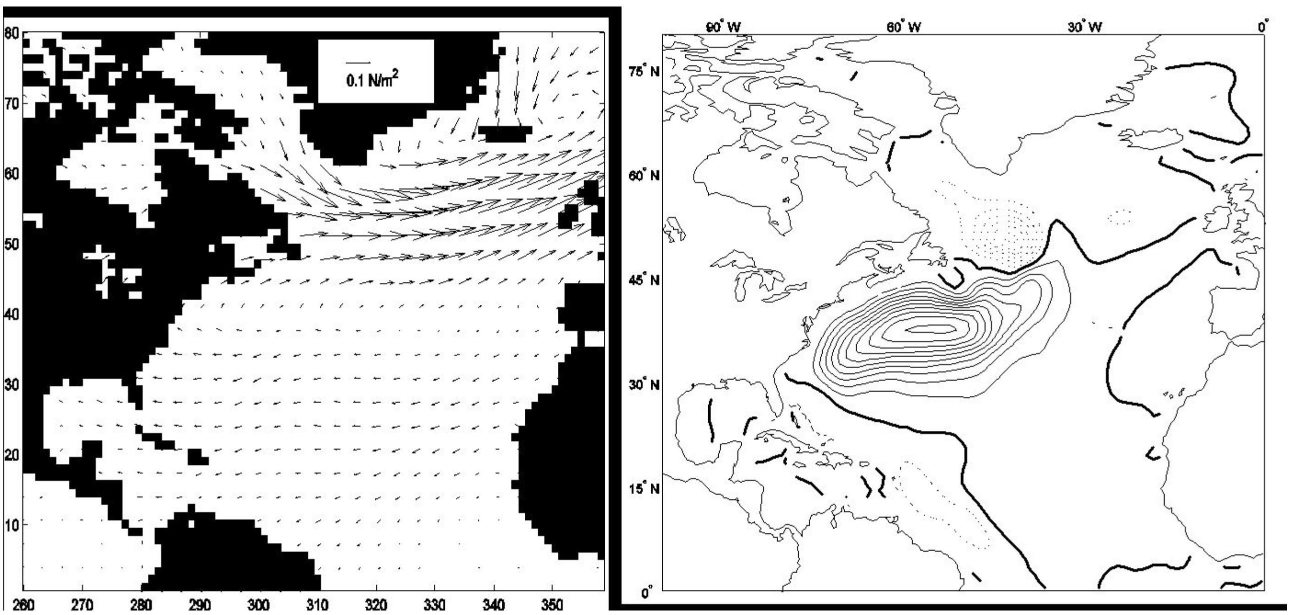

Figure 3: Left panel: Composite map of JFM wind-stress obtained as NAOI+ minus NAOI- difference. Right panel: EOF1 of barotropic streamfunction (in Sv). Dashed contour for negative values. Contour interval: 0.5 Sv.

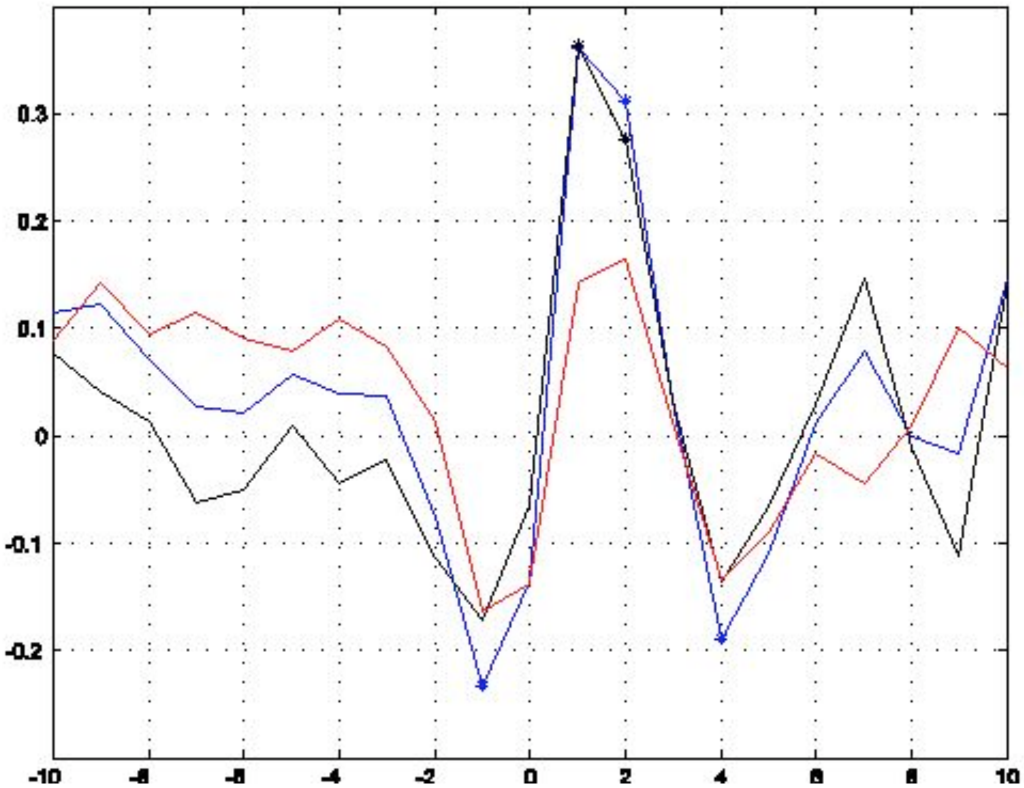

Figure 4: Lagged correlation between the NAOI and total (blue), gyre (black) and overturning (red) meridional heat transport. Stars indicate significant correlation at the 95% confidence level.

Land-Surface-Vegetation effects on climate: Application to Seasonal Predictions

Alessandri A.[1], S. Gualdi[1,2] and A. Navarra[1,2]

1: Centro Euro-Mediterraneo per i Cambiamenti Climatici
2: Istituto Nazionale di Geofisica e Vulcanologia

The first version of the INGV-CMCC Seasonal Predictions System (SPS) was implemented in the framework of the EU DEMETER project (http://www.ecmwf.int/research/demeter/). Since our engagement in DEMETER, we learned that CGCMs can be used with good skill in predicting the distribution of the SSTA (Sea Surface Temperature Anomalies) in the tropical Pacific at seasonal time scales, with much of the "memory" of the system residing in the upper ocean. As a consequence, it is crucial to determine the oceanic initial state as accurately as possible (Palmer et al., 2004). Furthermore, the prediction of the growing phase of strong El Niño events can be improved substantially using an high resolution atmospheric model (Gualdi et al., 2004). Further efforts at CMCC are currently devoted in trying to assess the impact on the SPS skill of [1] ocean initial conditions derived from higher resolution simulations, [2] atmospheric model resolution (T106 vs T42) and [3] Ocean model resolution (1/4° vs 2°).

A new version of the SPS (see the schematic diagram in figure 1) is currently under development (EU ENSEMBLES project framework; see http://www.ensembles-eu.org/ for more informations). The new SPS includes up to date versions of the Atmospheric and Oceanic models as well as Ocean data assimilation (Bellucci et al., 2006) and a newly developed Land Surface Model (SILVA: Surface Interactive Land VegetAtion; Alessandri, 2006). Considerable improvements in the skill of forecasting climate anomalies on seasonal-to-annual time scales are expected thanks to the use of the new SPS which will be ready for hindcasts production for March 2007.

A preliminary assessment of the land surface-vegetation impacts on Seasonal Predictions has been performed through the study of the sensitivity of to the Atmospheric component to the coupling with SILVA (Alessandri, 2006). The results indicate that the inclusion of SILVA in ECHAM substantially improves the Boreal Summer simulated surface fluxes and increases precipitation in areas covered with forests. Furthermore, a relationship between vegetation and rainfall interannual variability is identified and in close agreement with observations (13%), the model vegetation variability explains 12% of the rainfall variance over continents. The present work suggests the existence of a sort of "vegetation memory" influencing the climate system at seasonal time scales. In fact, both observations and model results show the same delayed vegetation effect on the large scale precipitation pattern which follows ENSO cycles (see figure 2).

Other studies have recently shown that the land surface could contribute to the predictability in the seasonal range forecasts through the "soil moisture memory" (e.g: Koster et al, 2004; Ferranti and Viterbo, 2006). This opens the discussion on how to suitably initialize land surface variables such as soil moisture content and/or vegetation state in our future Seasonal-to-annual prediction systems.

References:

Alessandri A., S. Gualdi, J. Polcher, e A. Navarra, 2007: Effects of Land Surface and Vegetation on the Boreal Summer Surface Climate of a GCM. J. Climate, 20 (2), 255-278.

Alessandri A., 2006: Effects of Land Surface and Vegetation Processes on the Climate Simulated by an Atmospheric General Circulation Model. Ph.D. Thesis.

Ferranti, L and P. Viterbo, 2006: The European Summer of 2003: Sensitivity to soil water initial conditions. J. Climate, 19 (15), 3659-3680

Koster et al, 2004: Realistic initialization of Land surface states: Impacts on subseasonal Forecast Skill. J. Hydrometeor., 5, 1049–1063.

Gualdi S., A. Alessandri, and A. Navarra, 2004: Impact of atmospheric horizontal resolution on ENSO forecasts. Tellus A, 57(3), 357-374.

Palmer, T. N. , A. Alessandri, U. Andersen, P. Cantelaube, M. Davey, P. Délécluse, M. Déqué, E. Diez, F. J. Doblas-Reyes, H. Feddersen, R. Graham, S. Gualdi, J.-F. Guérémy, R. Hagedorn, M. Hoshen, N. Keenlyside, m. Latif, A. Lazar, E. Maisonnave, V. Marletto, A. P. Morse, B. Orfila, P. Rogel, J.-M. Terres, M. C. Thomson, 2004: Development of a European Multi-Model Ensemble System for Seasonal to Inter-Annual Prediction (DEMETER). Bull. Amer. Meteor. Soc., 85, 853-872

Bellucci, A., S. Masina, P. Di Pietro, and A. Navarra, 2006: Using temperature-salinity relations in a global ocean implementation of a multivariate data assimilation scheme. Mon. Weather Rev. In press.

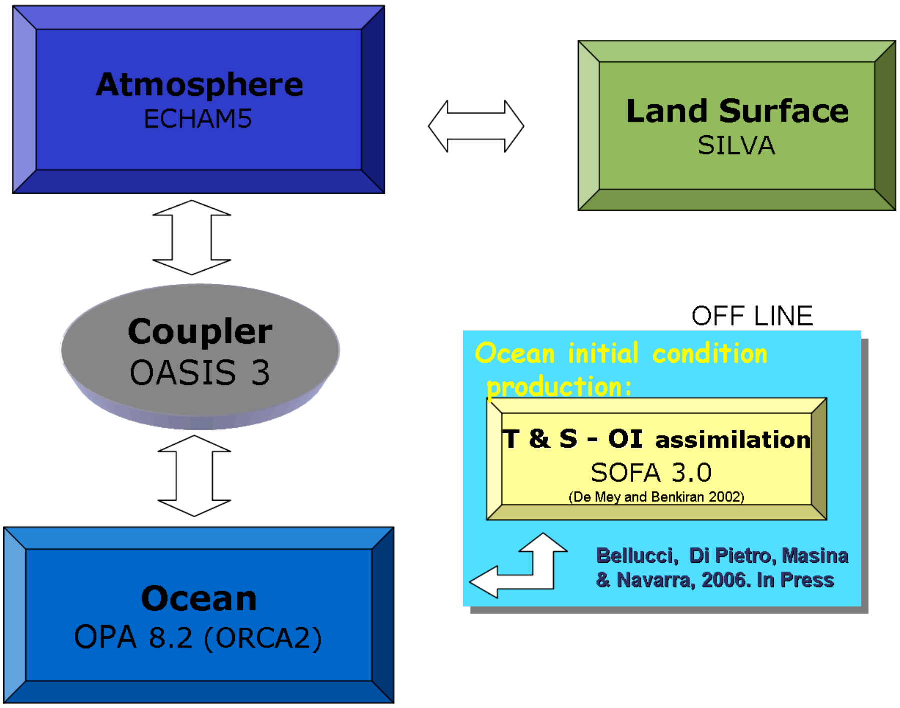

Figure 1: Schematic diagram of the new INGV-CMCC seasonal forecasting system (ENSEMBLES framework)

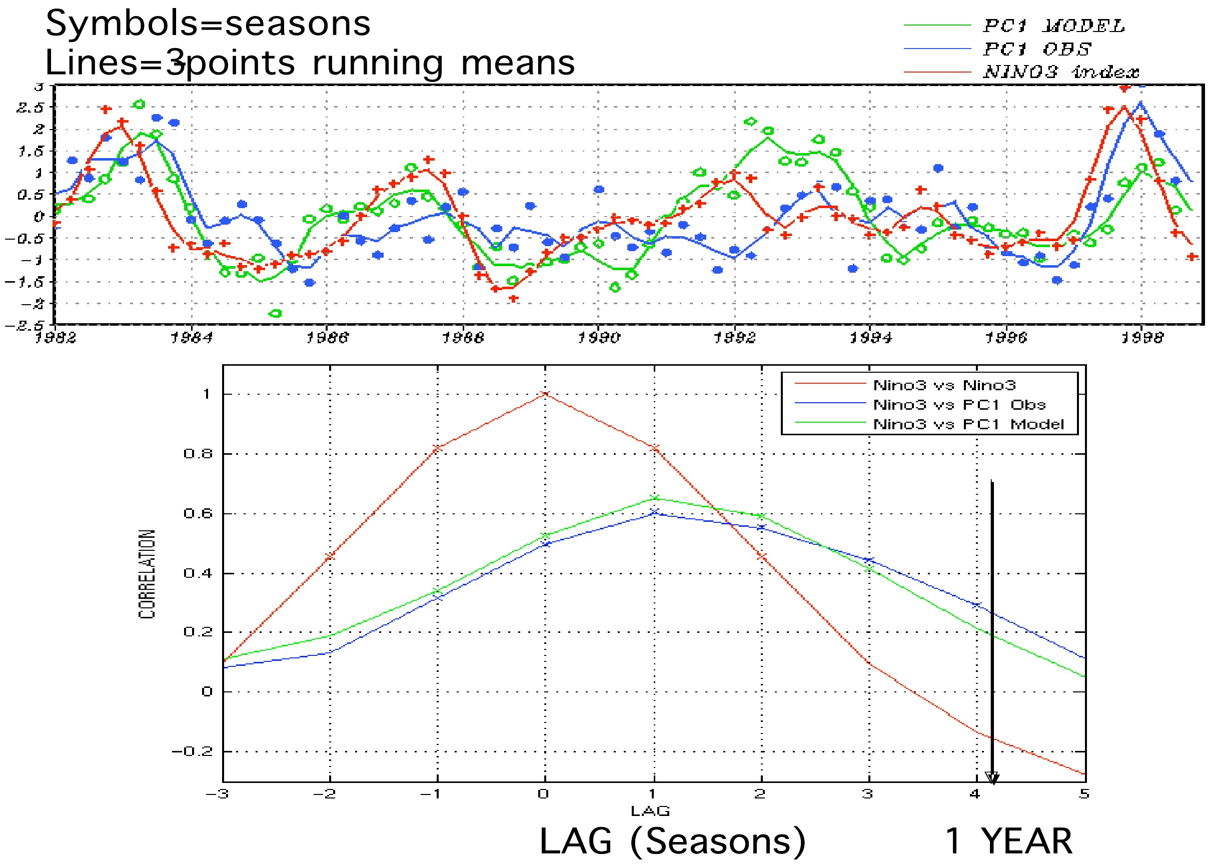

Figure 2: Upper panel: first normalized PCs of the precipitation forced manifold in the model (green) and in the observations (blue); in red is the NINO3 index. The anomalies have been divided by the standard deviation. Lower panel: Lagged correlations between the NINO3 index and the PCs reported in the upper panel. Red curve stands for the autocorrelation function of the NINO3 index. The marks indicate significant correlation at the 1% level.

The sensitivity of the Indo-Pacific climate variability to model resolution and CO2 concentration

Annalisa Cherchi[1,2]

1: Centro Euro-Mediterraneo per i Cambiamenti Climatici
2: Istituto Nazionale di Geofisica e Vulcanologia

The variability of the Indo-Pacific climate is dominated by two important large-scale phenomena: the Asian summer monsoon (ASM) and ENSO (El Nino Southern Oscillation). A set of experiments forced with observed SST has been performed with the Echam4 atmospheric GCM (Roeckner et al., 1996) at three different horizontal resolutions (T30, T42 and T106). These experiments have been used to study the sensitivity of the simulated ASM to the horizontal resolution. The ASM simulated by the Echam4 model is realistic, at least in terms of circulation and precipitation features (Cherchi and Navarra, 2006). An higher horizontal resolution is able to better represent some regional aspects of the precipitation field (e.g. the Western Ghats), however it can not represent the entire solution for the systematic error of the models (Cherchi and Navarra, 2006). The AMIP-type experiments have been compared with a set of experiments from the SINTEX coupled model (Gualdi et al., 2003a) to understand more on the importance of the air-sea interaction in the simulation of the ASM. The results from the coupled model experiments are realistic, somehow better but somehow worse than the AMIP-type experiments results. In particular, the coupled model tends to overestimate the SST in the Indian Ocean. In this condition, the SST gradient in the western part of the basin near Somalia is weak ans as a consequence the surface winds from the Indian Ocean towards India are less intense (Cherchi and Navarra, 2006). A new set of experiments has been performed with the atmospheric-only model forced with SST from the coupled model at the three horizontal resolutions. All the experiments have been integrated for 10 years. The differences between the results of the coupled model experiments and the new forced experiments are small. This result suggests that in the coupled model, the systematic errors in the SST are more crucial than the air-sea interaction in the simulation of the ASM (Cherchi and Navarra, 2006).

One of the main components of the ASM is the Indian summer monsoon (ISM). By means of a SINTEX coupled model experiment at high resolution we have analyzed the impact of Indian Ocean SST on the precipitation over India. The whole analysis is concentrated on the boreal summer (JJA mean). One third of the variability of the precipitation over India has been found to be influenced by SSTA in the Tropical Indian Ocean (Cherchi et al., 2006). That variance has been computed by means of the coupled manifold technique, which is a statistical method recently developed by Navarra and Tribbia (2005) which permits to analyze co-variation among two atmospheric fields. The Tropical Indian Ocean (TIO) is known to be influenced by the Tropical Pacific Ocean (TPO) (e.g.Wallace et al., 1998; Saji et al., 1999), so by means of the coupled manifold technique we have decomposed the SSTA of the TIO in one part which is forced from the variability of the TPO ('Forced SST') and a part which is free from that variability ('Free SSTA'). Total, forced and free TIO SSTA have been correlated with the Indian Monsoon Index (IMI) (fig.1), which is a dynamical index defined by Wang et al.(2001) as the difference of the zonal wind at 850mb between a region in the northern India and a region in the southern India. Comparing the results from the observations and the coupled model represented in fig.1, it may be argued that the model is able to reproduce the large-scale patterns observed. A strong bias in the model is the strong dipole-like dynamics simulated in the Tropical Indian Ocean (Cherchi et al., 2006). This may be linked to the systematic errors of the coupled model, like the strong feedback between winds, SST and thermocline slope simulated in the eastern tropical Indian Ocean (Fischer et al., 2005) and the weakness of the relationship between ENSO and the monsoon (Terray et al., 2005) simulated by the model.

ENSO and the monsoon are known to be negatively correlated (e.g. Webster and Yang, 1992), in particular a strong El Nino is generally followed by a weak monsoon the summer after the El Nino peak. The negative correlation is well captured by the atmospheric model when forced with prescribed SST (Cherchi and Navarra, 2006), as shown in fig.2. It is interesting to note that the negatively relationship weakens after 1976 (fig.2), as observed by Kumar et al. (1999).

The variability of the tropical Pacific sector has been analyzed by means of a set of experiment in which the CO2 concentration has been multiplied by a factor of 2, 4 and 16. The results have been compared with a control simulation. The experiments have been realized with the SINTEX coupled model, which simulates realistic features in the variability of both Pacific (Guilyardi et al., 2003) and Indian (Gualdi et al., 2003b) sectors. From the analysis of the main departures of the sensitivity experiments from the control simulation it is possible to have some insights on the main mechanisms involved in the ocean-atmosphere adjustment. A detailed analysis of the interannual variability of the Equatorial Pacific Ocean reveals that when the CO2 concentration increases by about 2 and 4 times with respect to the control simulation the El Nino oscillation intensifies, on the other hand in the experiment with 16 times the present day value of CO2, the El Nino-like oscillation decreases in intensity and the mean state simulated suggests the possibility of the establishment of permanent El Nino conditions.

References:

Cherchi A., and A. Navarra, 2006: Sensitivity of the Asian summer monsoon to the horizontal resolution: Differences between AMIP-type and coupled model experiments, *Climate Dynamics*, DOI: 10.1007/s00382-006-0183-z.

Cherchi, A., S. Gualdi, S. Behera, J.J. Luo, S. Masson, T. Yamagata and A. Navarra, 2006: The influence of Tropical Indian Ocean SST on the Indian summer monsoon. Accepted on J. Climate.

Fischer, A.S., P. Terray, E. Guilyardi, S. Gualdi and P. Delecluse, 2005: Two indipendent triggers for the Indian Ocean Dipole/Zonal Mode in a coupled GCM; *J. Climate*, **18**, 3428-3449.

Gualdi, S., A. Navarra, E. Guilyardi and P. Delecluse, 2003a: Assessment of the tropical Pacific climate in the SINTEX CGCM, *Annales Geophysicae*, **46**, 1-26.

Gualdi, S., E. Guilyardi, A. Navarra, S. Masina and P. Delecluse, 2003b: The interannual variability in the tropical Indian Ocean as simulated by a CGCM; *Climate Dynamics*, **20**, 567-582.

Guilyardi, E., P. Delecluse, S. Gualdi and A. Navarra, 2003: Mechanisms for ENSO phase change in a coupled GCM; *J. Climate*, **16**, 1141-1158.

Kumar, K:K., B. Rajagopalan and M.A. Cane, 1999: On the weakening relationship between the Indian monsoon and ENSO; Science, 284, 2156-2159.

Roeckner, E., K. Arpe, L. Bengtsson, M. Cristoph, M. Claussen, L. Dumenil, M. Esch, M. Giorgetta, U. Schlese and U. Schulzweida, 1996: The atmospheric general circulation model ECHAM4: Model description and simulation of present-day climate. Max-Planck Institut fur Meteorologie, Report. n 218, Hamburg, 86 pp.

Saji, N.H., B.N. Goswami, P.N. Vinaychandran and T. Yamagata, 1999: A dipole mode in the tropical Indian Ocean, *Nature*, **401**, 360-363.

Terray, P., E. Guilyardi, A.S. Fischer and P. Delecluse, 2005: Dynamics of the Indian monsoon and ENSO relationships in the SINTEX global coupled model; *Climate Dynamics*, **24**, 145-168.

Wallace, J.M, E.M. Rasmusson, T.P. Mitchell, V.E. Kousky, E.S. Sarachik and H. von Storch, 1998: On the structure and evolution of ENSO-related climate variability in the tropical Pacific: Lessons. *J. Geophys. Res.*, **103**(C7), 14 241-14 260.

Wang, B., R. Wu and K.M. Lau, 2001: Interannual variability of the Asian summer monsoon: Contrasts between the Indian and the Western North Pacific-East Asian monsoons; *J. Climate*, **14**, 4073-4090.

Webster, P.J., and S. Yang, 1992: Monsoon and ENSO: Selectively interactive systems; *Q. J. Roy. Meteor. Soc.*, **118**, 877-926.

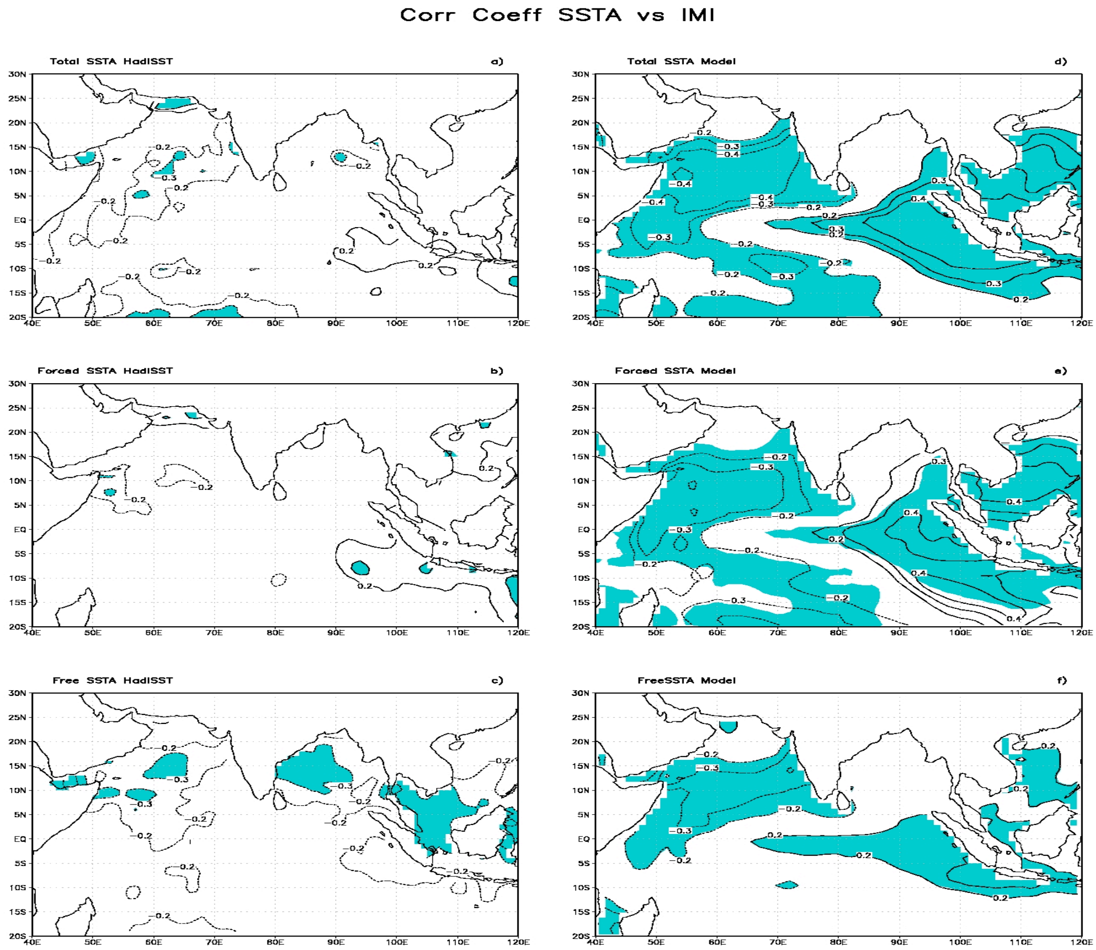

Figure 1: Correlation coefficients between IMI and total, “forced” and “free” SST anomalies in the TIO for the HadISST dataset (a,b,c) and for the coupled model results (d,e,f). Values shaded are significant at 95%.

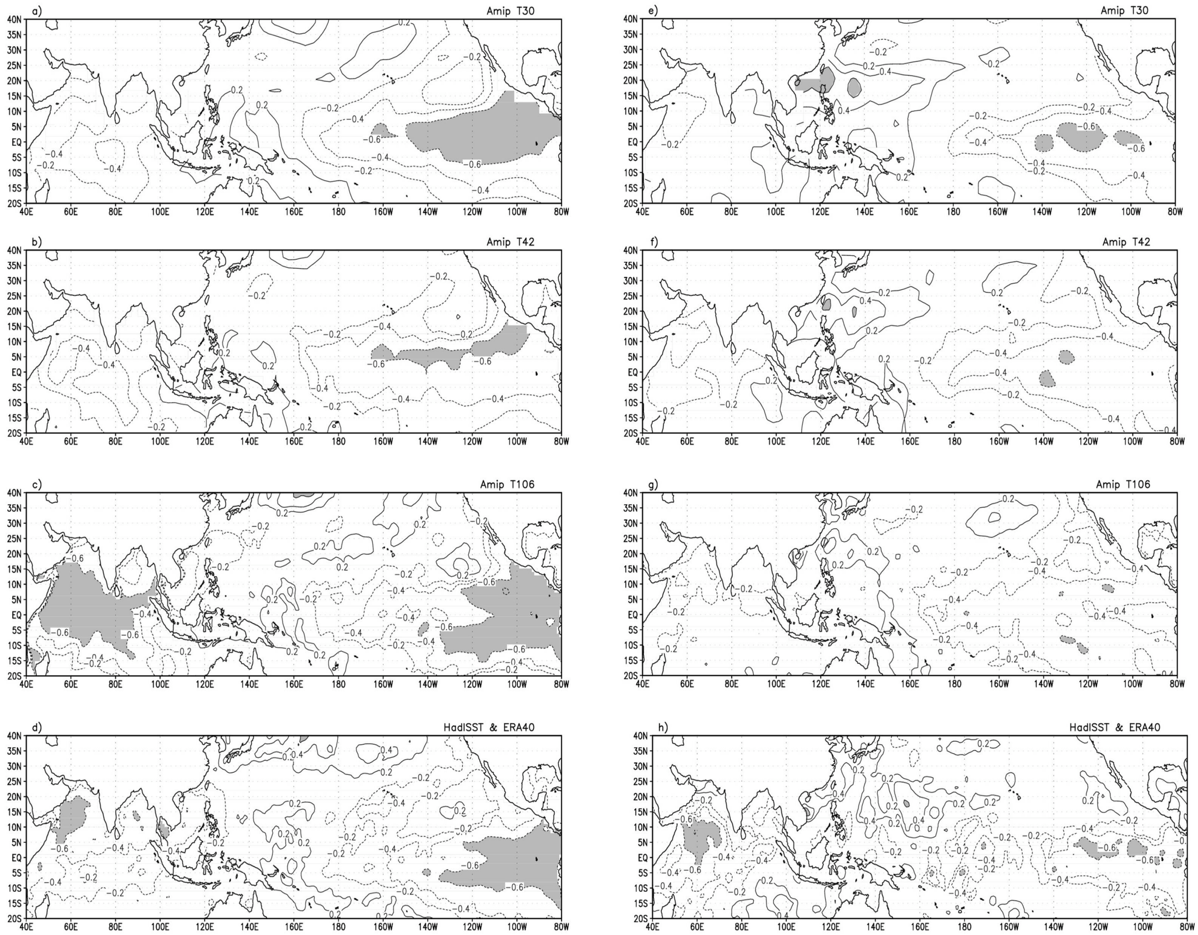

Figure 2: Correlation maps of JJA mean SST and DMI for the Echam4 Amip-type experiments and the reanalysis, before 1976 (left panels) and after 1976 (right panels). Shaded values are lower than -0.6 and higher than 0.6.

The CMCC/INGV Earth System Model: Configuration and Preliminary Results.

E. Manzini[1,2], P.G. Fogli[1], M. Vichi[1,2], A. Alessandri[1], S. Gualdi[1,2], S. Masina[1,2], A. Navarra[1,2], L. Patara[2], and E. Scoccimarro[2].

1: Centro Euro-Mediterraneo per i Cambiamenti Climatici
2: Istituto Nazionale di Geofisica e Vulcanologia

Introduction:

The need to simulate the evolution of the atmospheric CO2 consistently with climate variations and climate change has motivated the recent development of the Earth System Models (ESMs) of the carbon cycle. An ESM that aims at simulating the carbon cycle in a comprehensive way consists of a physical core (atmosphere-ocean coupled general circulation model including sea ice) coupled to a model of the carbon cycle. Therefore, the three dimensional evolution of carbon is simulated in an ESM, together with the evolution of the carbon sources and sinks over land (vegetation model) and in the ocean (biogeochemical model). The coupling with the climate occurs at the surface (the vegetation and ocean influence on the surface exchange of biophysical fluxes) and through the radiative forcing implied by the changing CO2 atmospheric concentration.

Results are presented for the ESM in development at the CMCC/INGV. The physical core model of the CMCC/INGV ESM is a newly coupled atmosphere ocean general circulation model and it is composed by the ECHAM5 atmosphere model (Roeckner et al 2006), the OPA8.2 ocean model (Madec et al 1998) and the LIM sea-ice model (Timmermann et al 2005). The coupler OASIS3 (Valcke et al 2004) is used to exchange the relevant fields. The previous experience established for the construction of the SINTEX-G model (Gualdi et al 2003) has been crucial for establishing the base framework for the upgrading of the physical core. The physical core model (hereafter EOL model for brevity) has been tested at the T31L19 and T63L31 resolutions for the atmospheric component and with the ORCA2 resolution for the ocean component. The carbon cycle module includes the SILVA terrestrial vegetation model (Alessandri 2006) and the PELAGOS marine biogeochemistry model (Vichi et al 2007a,b).

Results:

Simulations of the EOL model have been performed for present conditions and have demonstrated that the coupled model is stable for at least several decades, at both the resolutions tested. In the following, selected results are reported for a 100 year simulation performed with the EOL model at T31L19. Work on the coupling of the carbon cycle is in progress.

Surface air temperature

The time evolution of the global annual mean surface air temperature from the EOL model during the present climate simulation is shown in Figure 2.

The coupled model is initalized with the Levitus (1982, updated) thermal structure. After the initial adjustement, the surface air temperature tends to stabilize at about 1 – 1.5 ^{o}C above the observed climatological value of the last 40 years, given by the ERA40 reanalysis. This warm bias may be explained by the lack of sulphate aerosol in the current climate simulation. During the last 50 years, there still is a relatively small tend (+0.4 ^{o}C/century) in the surface air temperature, typical for non-flux adjusted coupled models.

Sea-ice

The mean sea ice cover for January-February-March (JFM) and July-August-September (JAS) for the Artic is shown in Figure 3.

Figure 3 shows that the EOL model captures the seasonality of the Arctic sea-ice cover in reasonable agreement with satellite observations. However, in the North Western Pacific the sea-ice distribution along the Asian coast is underestimated in winter. This bias in sea-ice is related to a warm bias in the sea surface temperature between 30^{o}N and 60^{o}N in the Western Pacific. In the Antarctic, the sea-ice cover shows the seasonal variation, however small, and is in general underestimated in both summer and winter (not show).

Precipitation

The mean precipitation for January-February-March (JFM) and July-August-September (JAS) is shown in Figure 4.

The seasonal evolution of the precipitation at middle latitudes is captured by the EOL model: High precipitation along the Northern hemisphere storm tracks in JFM and along 50^{o}S in JAS. In the tropics, the seasonal shift of the Intertropical Convergence Zone (ITCZ, the region of higher precipitation) is well simulated. The South Pacific Convergence Zone (SPCZ) weakens from JFM to JAS, as observed. However, in JFM the SPCZ extends too far eastward in the South Pacific, the manifestation of the "double ITCZ" bias typical to virtually all coupled models. Moreover, the precipitation is globally overestimated in the EOL model.

Acknowledgment: Part of this work has been funded by the ENEMBLES Integrated Project of the European Commission.

References:

Alessandri A. 2006: Effects of Land Surface and Vegetation Processes on the Climate Simulated by an Atmospheric General Circulation Model, PhD thesis, Alma Mater Studiorum University of Bologna, Italy.

Gualdi, S., E. Guilyardi, P. Delecluse, S. Masina and A. Navarra, The interannual variability in the tropical Indian Ocean as simulated by a CGCM, Clim. Dynam., 20, 567-582, 2003.

Levitus, S., T.P. Boyer, M.E. Conkright, T. O'Brien, J. Antonov, C. Stephens, L. Stathoplos, D. Johnson, & R. Gelfeld (1998) World Ocean Database 1998 Volume 1: Introduction. NOAA Atlas NESDIS 18, U.S. Government Printing Office, Washington, D.C.

Madec, G., P. Delecluse, M. Imbard, and C. Lévy, 1998: OPA 8.1 Ocean General Circulation Model reference manual. Note du Pôle de modélisation, Institut Pierre-Simon Laplace, N°11, 91pp.

Roeckner, E., R. Brokopf, M. Esch, M. Giorgetta, S. Hagemann, L. Kornblueh, E. Manzini, U. Schlese, and U. Schulzweida, 2006: Sensitivity of simulated climate to horizontal and vertical resolution in the ECHAM5 atmosphere model. J Climate, 19, 3771-3791.

Timmermann, R., H. Goosse, G. Madec, T. Fichefet, C. Ethé, and V. Dulière, 2005: On the representation of high latitude processes in the ORCA-LIM global coupled sea ice ocean model, Oc. Model., 8, 175-201.

Valcke S., A. Caubel, R. Vogelsang, and D. Declat, 2004: OASIS3 User Guide (oasis3_prism_2-4). PRISM Report No 2, 5th Ed. CERFACS, Toulouse, France. 60 pp.

Vichi M., N. Pinardi and S. Masina, 2007a: A generalized model of pelagic biogeochemistry for the global ocean ecosystem. Part I: Theory. J. Marine Systems, 64(1-4), 89-109.

Vichi M., S. Masina and A. Navarra, 2007b: A generalized model of pelagic biogeochemistry for the global ocean ecosystem. Part II: numerical simulations. J. Marine Systems, 64(1-4), 110-134.

Xie, P. and P.A. Arkin, 1997: Global Precipitation: A 17-year monthly analysis based on gauge observations, satellite estimates, and numerical model outputs, Bulletin of the American Meteorological Society, 78, 2539-2558.

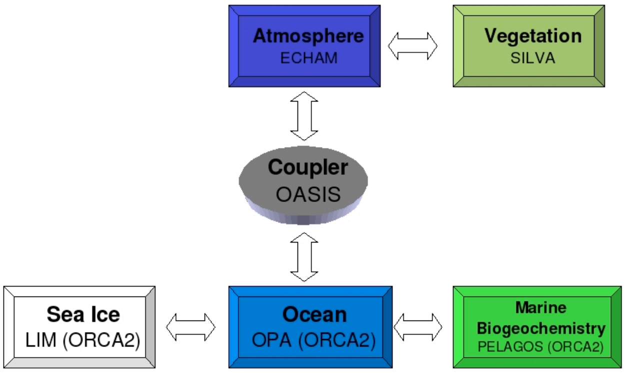

Figure 1: Structure of the CMCC/INGV Earth System Model.

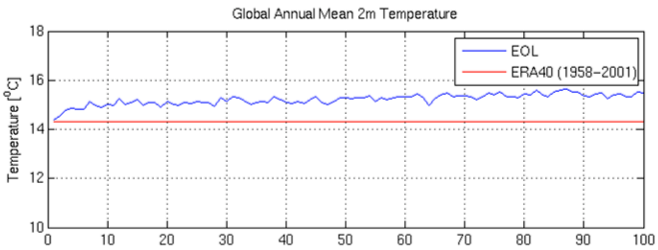

Figure 2: Global annual mean of the surface air temperature from the EOL model (bleu) and the ERA40 (red, climatological mean 1958-2001).

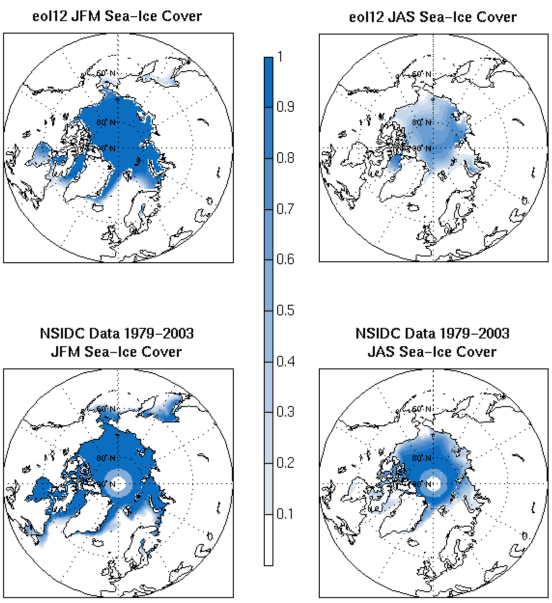

Figure 3: Mean sea-ice cover (%) for JFM at left and JAS at right. EOL model results (average over the last 50 years of the simulation) at top, NSIDC satellite data at bottom.

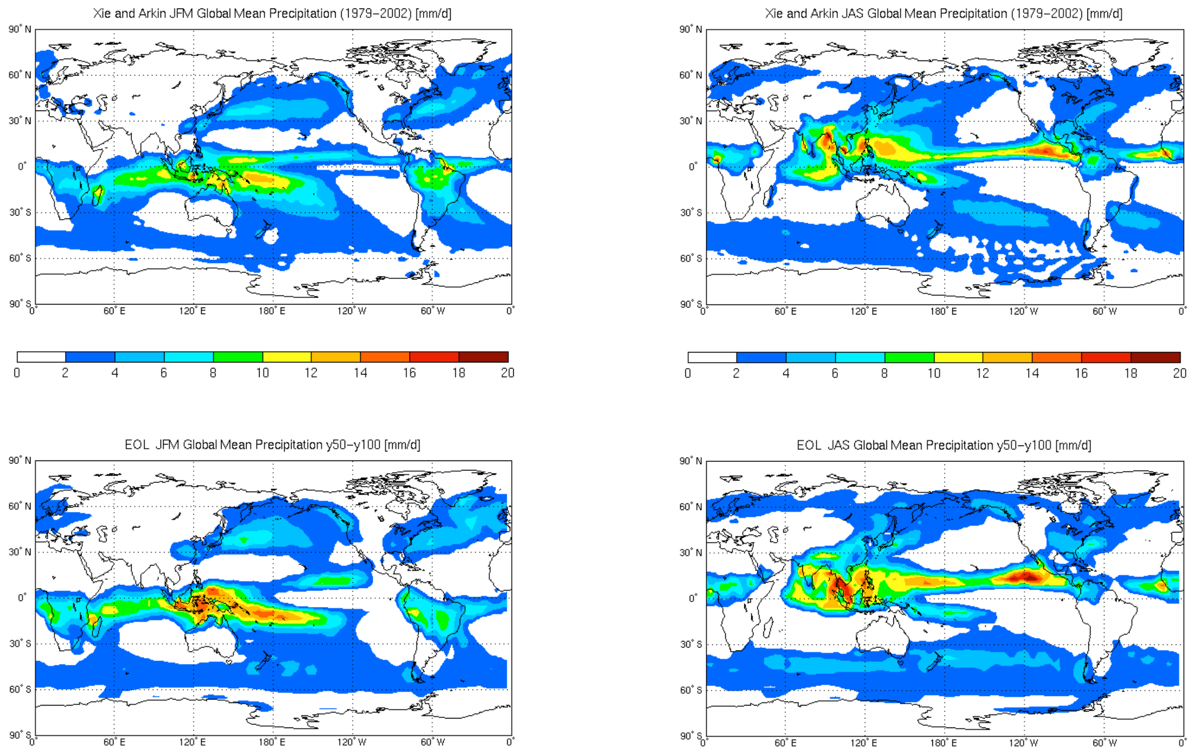

Figure 4: Mean Precipitation for JFM at left and JAS at right. Observations (Xie and Arkin, 1997 updated) are at top and the EOL model (average over the last 50 years of the simulation) at bottom.

Physical-biogeochemical interactions across scales in the equatorial Pacific

M Vichi[1,2], PG Fogli[1], L Patara[2], E Manzini[1,2], S Masina[1,2], A Bellucci[1], E Scoccimarro[2], S Gualdi[1,2], A Navarra[1,2]

1: Centro Euro-Mediterraneo per i Cambiamenti Climatici
2: Istituto Nazionale di Geofisica e Vulcanologia

Marine ecosystems are major components of the Earth System and contribute to the regulation of atmospheric CO_2. The most productive regions of the oceans (namely, the North Atlantic and subarctic Pacific, the Southern Ocean and the major upwelling areas) are responsible for most of the air-sea exchange of inorganic carbon and for the likely organic carbon export to the deep ocean. The high concentration of phytoplankton biomass is also responsible for the attenuation of the penetrating irradiance in the water column, which modifies the thermal budget of the surface ocean. Numerical experiments have shown the impact of the different parameterizations of light attenuation on the results of OGCMs (Murtugudde et al 2002; Marzeion et al 2005, Wetzel et al 2006; Sweeney et al. 2006, Nakamoto et al. 2001; Shell et al. 2002; Manizza et al 2005), indicating that the induced different distributions of heat in the vertical and horizontal dimensions can lead to different physical patterns.

This is particularly true in the equatorial Pacific, and some recent papers have focused the analysis on this specific region where the coupling between atmosphere and ocean determines the ENSO variability. ENSO is a large-scale phenomenon, while phytoplankton activity is limited to the first 100 m of the water column and with limited spatial coverage mostly confined to the eastern part. Published simulation results hint at a marked impact of phytoplankton-driven light attenuation, showing in some cases an increase of SST and in some others a decrease, with related modifications of the mixed layer depth. However little emphasis is provided in the papers on the spatial distribution of phytoplankton and how it affects the general circulation because it is assumed that the attenuation mostly occurs in the surface layer.

The heating effect of phytoplankton has been studied in a coupled Earth System Model which incorporates a comprehensive marine biogeochemistry model. The ESM structure is outlined in Manzini et al. (this volume). The biogeochemistry model is PELAGOS (PELagic biogeochemistry for Global Ocean Symulations), which is fully described in Vichi et al., 2007a. PELAGOS is a global ocean implementation of the Biogeochemical Flux Model (BFM, developed in the MFSTEP EU-project, http://www.bo.ingv.it/bfm) which solves the biogeochemical cycles of major pelagic constituents with an on-line coupling with the OPA (ORCA2) OGCM. Climatological results of the forced simulations are discussed in Vichi et al. (2007b).

The ESM was run for 80 years after a spinup of 40 years with two different configurations: 1) light attenuation is parameterized with the standard coefficients derived from case I waters (Paulson and Simpson, 1976; BLUE ocean); 2) attenuation is related to total chlorophyll concentration with a mean specific coefficient of 0.03 m^2 $mgChl^{-1}$ (GREEN ocean).

Fig. 1 shows a comparison of the simulated annual vertical distribution of Chl (meridional section at 110W) with the data from the World Ocean Atlas 2001 (WOA01). The subsurface chlorophyll maximum is reasonably simulated by the model with a discrepancy of less than 20 m and The asymmetry in the subsurface latitudinal distribution is also well represented while the surface gradient is smoother than observed.

The computed average attenuation coefficient over the first 100 m is slightly higher than the constant BLUE-ocean value but the differences in the mean surface and vertical temperature distributions over the 80 years are significant (Fig. 2, p>0.99). The GREEN ocean is slightly colder at surface and the highest cooling is found in the subsurface convergence layer around 5-10 degrees south/north.

Despite the positive (although weak) heating rate induced by chlorophyll absorption, the dynamical large-scale response tends to contrast the local heating and the equilibrium solution is characterised by an overall cooling of the equatorial Pacific with an increase of the divergence in the western part. The atmosphere participates to this equlibrium with an increase of the western portion of the Walker cell and a slight decrease of the intertropical converge in the eastern Pacific (not shown, cfr. Shell et al., 2002).

Model results show that the dynamical response induced by the local heat absorption is in agreement with the theoretical studies by Edwards et al. (2004). Fig. 3 shows the induced perturbed velocities (u, v and w components) together with the vertical chlorophyll distribution. Biologically-induced currents are weaker than the general circulation (<5%), yet are correlated with phytoplankton gradients as described by Edwards et al. Recirculation cells are found at the meridional margins, especially on the southern flank where the pattern is not complicated by the subsurface maximum at 9N.

The results hint at a role of phytoplankton in the dynamics of the first 300 m, because the basin-scale induced dynamical response is higher than the local heating rate (result not shown). This implies that the structure of phytoplankton distribution should be carefully considered and we cannot just assume that pigment absorption occurs in the surface layers.

However, given the high uncertainty in the definition and parameterization of phytoplankton optical properties, it is difficult to draw major conclusions at this stage on the role of autotrophs in the heat balance of the equatorial Pacific. The sensitivity of this climate model to this component at these scales is comparable to or even lower than the one induced by other factors (e.g. cloud parameterization, momentum coupling at the air-sea interface, etc). A critical intercomparison study of the different parameterizations and assumptions need to be undertaken as soon as computational power allows for massive ESM simulations.

References:

Edwards AM, Wright DG, Platt T. Biological heating effect of a band of phytoplankton. J. Marine systems 49 (1-4), pp 89-103, 2004

Manizza M, C. Le Quéré, A.J. Watson, E.T. Buitenhuis. Bio-optical feedbacks among phytoplankton, upper ocean physics and sea-ice in a global ocean. Geophys Res Lett 32(5), 2005.

Marzeion B, A. Timmermann, R. Murtugudde, F. Jin, 2004. Biophysical feedbacks in the tropical Pacific. J Climate 18 (1), 2005.

Murtugudde R, J. Beauchamp, C.R. McClain, M. Lewis, A.J. Busalacchi. Effects of penetrative radiation on the upper tropical ocean circulation. J Climate 15 (5), 2002.

Nakamoto S, S.P. Kumar, J.M. Oberhuber, J. Ishizaka, K. Muneyama, R. Frouin. Response of the equatorial Pacific to chlorophyll pigment in a mixed layer isopycnal ocean general circulation model. Geophys Res Lett 28 (10), 2001.

Shell KM, R. Frouin, S. Nakamoto, R.C.J., Somerville. Atmospheric response to solar radiation absorbed by phytoplankton. J Geophys Res 108 (D15), 2003.

Vichi M., N. Pinardi and S. Masina. A generalized model of pelagic biogeochemistry for the global ocean ecosystem. Part I: Theory. J. Marine Systems, 64(1-4), pp 89-109, http://dx.doi.org/10.1016/j.jmarsys.2006.03.006, 2007a .

Vichi M., S. Masina and A. Navarra. A generalized model of pelagic biogeochemistry for the global ocean ecosystem. Part II: numerical simulations. J. Marine Systems, 64(1-4), pp 110-134 http://dx.doi.org/10.1016/j.jmarsys.2006.03.014, 2007b.

Wetzel P, Maier-Reimer E, Botzet M, Jungclaus J, Keenlyside N, Latif M. Effects of ocean biology on the penetrative radiation in a coupled climate model. J. of Climate 19 (16), pp: 3973-3987, 2006

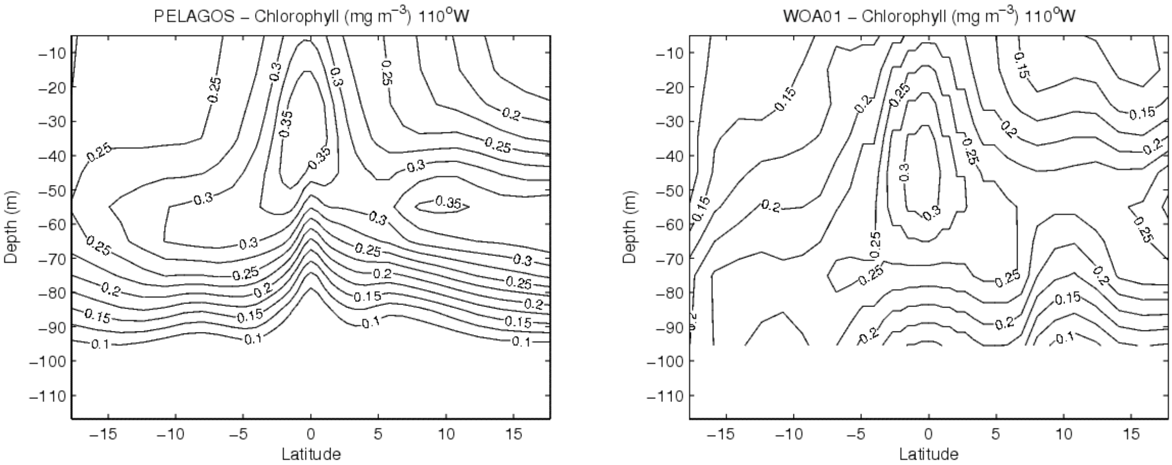

Figure 1: Vertical annual mean distribution of chlorophyll concentration at 110W. (a) simulated; (b) observed, WOA01

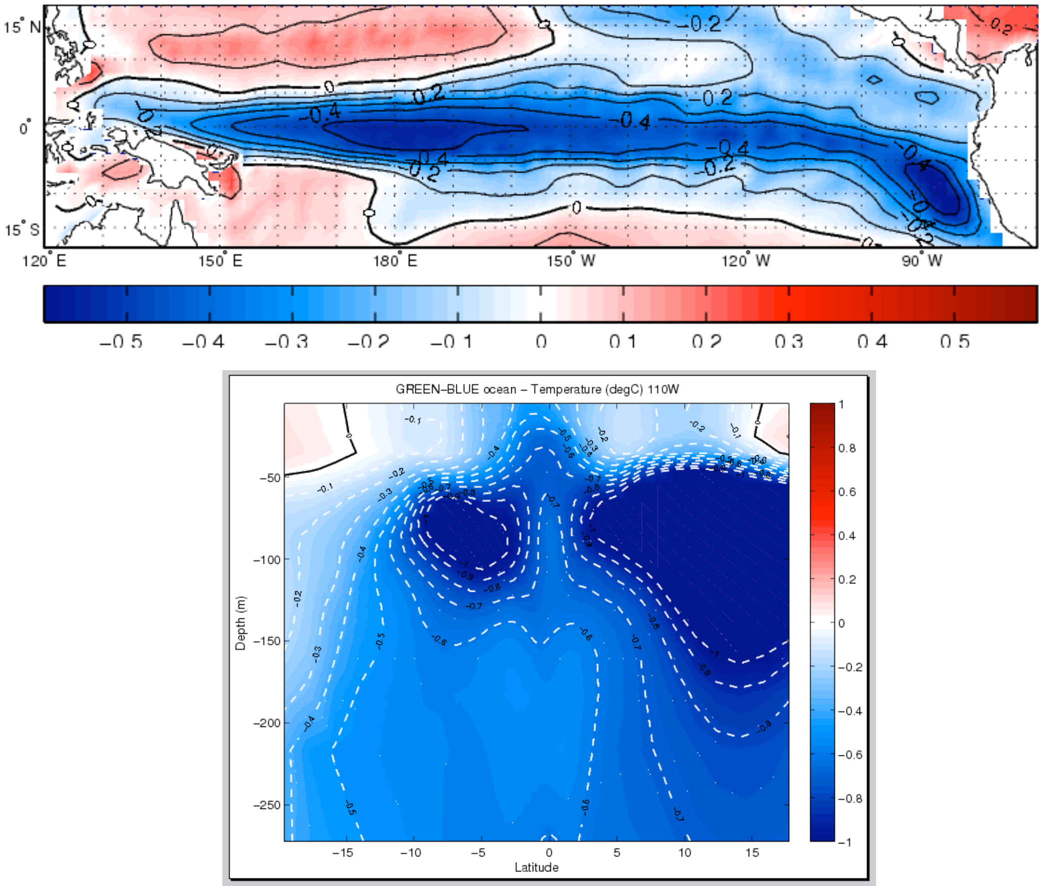

Figure 2: GREEN-BLUE ocean. Differences in the (a) SST annual mean and (b) in the first 300 m at 110W (deg C).

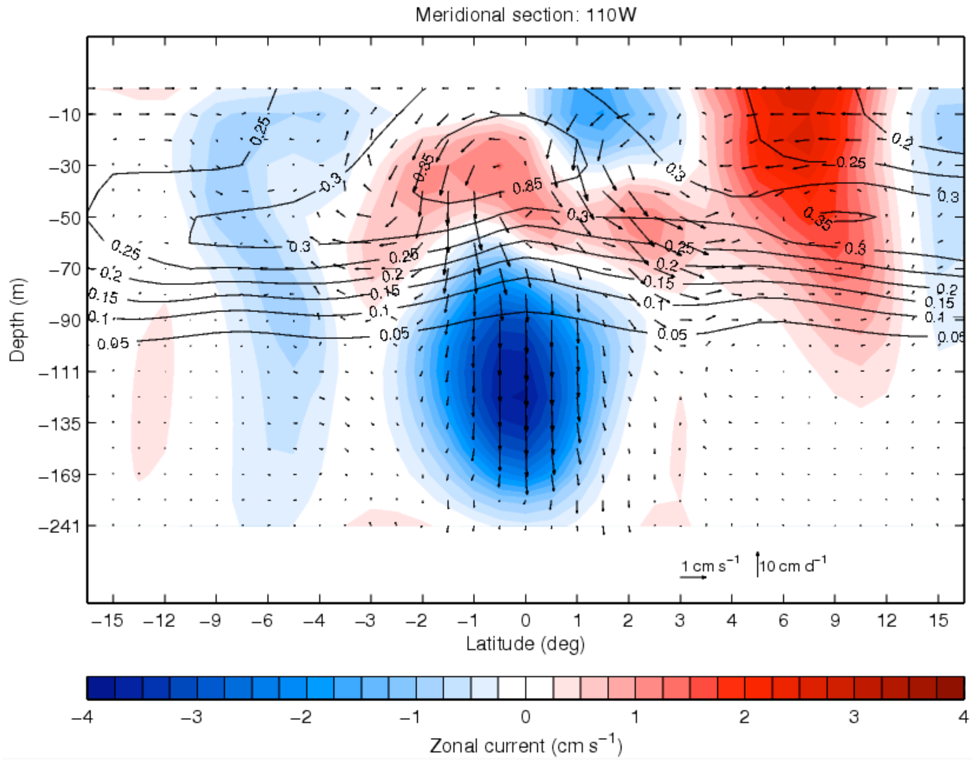

Figure 3: Biologically-induced currents (GREEN-BLUE) and chl vertical distribution in the meridional section at 110W. Vectors: vertical and meridional currents; shading: zonal currents; contours: chlorophyll concentration (mg m-3).

Modelling the global atmosphere at high horizontal resolution

E. Roeckner[1], L. Bengtsson[1,2], M. Esch[1], K. Hodges[2], J.-J. Luo[3], H.Wan[1], T. Yamagata[3,4]

1: Max Planck Institute for Meteorology, Hamburg, Germany
2: Environmental Systems Science Centre, Reading, UK
3: Frontier Research Center for Global Change, JAMSTEC, Yokohama, Japan
4: The University of Tokyo, Tokyo, Japan

The impact of increased resolution on simulated climate is a long-standing issue (e.g. Roeckner et al., 2006). In the first part of this study, the simulated seasonal climate obtained at very high horizontal resolution (ECHAM5 T319, corresponding to a grid spacing of about 40 km at the equator) is compared to ERA40 reanalyses and to that at lower resolution (ECHAM5 T106), corresponding to a grid spacing of about 110 km at the equator). It is found that (i) both simulations are in good agreement with ERA40 data und (ii) that the improvements at T319 are rather modest compared to T106 (both models use the same number of levels: 31). Also, the large-scale precipition patterns simulated by these models are rather similar and in good accordance to observations, except over the oceans where both models produce generally too much precipitation.

In the second part, the development of a baroclinic wave in an idealized model setup was studied. Starting from a balanced initial state, a small disturbance was introduced at northern midlatitudes triggering an unstable baroclinic wave that reached its mature state after 9 days. This case study has been proposed by Jablonowsky and Williamson (2006) for testing the convergence properties of dynamical cores. It is shown that the wave is developing at all resolutions tested (T42 to T319), but the frontal structures are becoming sharper as the resolution is increased up to T319. However, the differences between T159, T255 and T319 are small. In a full model, the sharpening of the frontal structures at high resolution is expected to lead to more extreme rain events.

In the third part, the impact of horizontal resolution on the simulation of tropical cyclones has been assessed. The simulations include an AMIP-type experiment performed at moderately high resolution (T159, corresponding to a grid distance of about 80 km at the equator) and two pairs of time slice experiments at T213 and T319 resolution, respectively, with SST's and sea ice interpolated from coupled model experiments (T63) for the present-day climate (end of the the 20th century) and for the future climate (end of 21st century according to an SRES A1B scenario).

The following criteria were used for the identification of tropical cyclones (based on a comparison of observed events and those obtained from the ECMWF operational analyses): Vorticity at 850 hPa > $6x10^{-5}$ s^{-1}; vorticity at 850 hPa at least $6x10^{-5}$ s^{-1} larger than at 250 hPa (defining the warm core) and lifetime (according to these requirements) of at least 24 hours. Using these criteria, the cyclone tracks and the frequency distribution for different regions have been compared to the observed record as well to ERA40 and JRA25 reanalyses. It is found that (i) the total number is overestimated by the model, (ii) the number of cyclones reaching hurricane strength (surface wind velocity > 33 ms-1) is realistic, but (iii) the number of strong ones (> 50 ms^{-1}) is severely underestimated (72 instead of 346 observed). In both reanalyses, the total number is about correct, but both reanalyses fail to reproduce the strong ones with wind speeds exceeding 50 ms^{-1} (only 1 in ERA40 and 2 in JRA25).

At higher horizontal resolution (T213 and, in particular, T319) the frequency distribution is becoming more realistic, i.e. total the number of weaker storms is smaller, whereas the number of stronger ones is substantially higher. Also, the tail of the distribution is extended to higher wind speeds reaching, for example, more than $80 ms^{-1}$ at T319 resolution.

In response to global warming, the total number of tropical cyclones is decreased in all regions under investigation (northern hemisphere only). However, the number of hurricane-strength cyclones is either unchanged or increased (East Pacific and Atlantic Ocean). Moreover, in these regions, the tail of the frequency distribution is extended to higher wind speeds. These results are found in both experiments (T213 and T319) and are also consistent with those obtained by Oouchi et al. (2006) at even higher resolution (20 km grid).

References:

Jablonowsky, C. and D.L. Williamson, 2006: A baroclinic instability test case for atmospheric model dynamical cores. Q. J. R. Meteorol. Soc., 128, doi: 10.1256/qj.06.n

Oouchi, K. et al., 2006: Tropical cyclone climatology in a global-warming climate as simulated in a 20 km mesh global atmospheric model: Frequency and wind intensity analyses. J. Meteorol. Soc. Japan, 84, 259-276.

Roeckner, E. et al., 2006: Sensitivity of simulated climate to horizontal and vertical resolution in the ECHAM5 atmosphere model. J. Climate, 19, 3771-3791

Sensitivity of the tropospheric temperature and circulation to the dynamics of the stratosphere

**M. A. Giorgetta[1] , M. Esch[1], I. Fischer-Bruns[1], E. Manzini[2],
W. A. Müller[1] and E. Roeckner[1]**

1: MPI-M Hamburg
2: CMCC/INGV Bologna

Introduction:

This work addresses two major questions: 1. what is the role of the stratospheric dynamics for the climate in the stratosphere? 2. is the coupling of atmosphere and ocean important to understand the interaction of the stratosphere and troposphere? Several aspects of these questions have been addressed already in observed or analyzed fields as well as in numerical models. The motivation for this specific work is to investigate both questions in the context of numerical climate simulations with coupled atmosphere ocean general circulation models, as typically employed for studies of the variability in the 20th century or of climate projections for the future. Specifically this work makes use of a pair of atmospheric models with identical representations of the troposphere and the stratosphere below 100 hPa, but different representations of the atmosphere above 100 hPa.

While one AGCM has a low top at 10 hPa the other model extends to the mesosphere to 0.01 hPa, and consequently the dynamics in the stratosphere differs due to differently acting dissipation mechanisms.

In the low top model the increased dissipation below the top acts close to the tropopause, while in the high top model the stratospheric winds depend on resolved dynamics, parameterized gravity wave drag, but not directly on the increased dissipation that is necessary close to the top in the mesosphere.

Differences in the stratospheric circulation, in its mean and variability, are therefore expected and do occur. If the stratospheric circulations differ in Northern hemisphere winter or Southern hemisphere spring, the dynamical coupling of the high latitude circulations in stratosphere and troposphere could lead to different tropospheric responses to the changed representations of the stratospheric circulation in the low and high top model.

Using this pair of AGCMs in otherwise identical experiments, differences between the tropospheres of both experiments must be related to different interactions between the tropospheres and respective stratospheres. This will be investigated to address question 1. Employing this pair of models in experiments with prescribed lower boundary conditions for sea surfaces or with coupling to an OGCM will allow the investigation of the coupling on the troposphere stratosphere interaction. This will be used for question 2.

Models:

The model used here is the generic ECHAM5 atmospheric GCM and the coupled ECHAM5/MPIOM atmosphere ocean GCMs. The AGCM is used in two vertical grid configurations, which have identical vertical grids from the surface to 100 hPa:

ECHAM5 in its standard resolution for tropospheric applications:

- horizontal resolution = T63
- vertical grid: 31 levels, 26 levels from surface to 100 hPa, top full level = 10 hPa.

MAECHAM5 is the middle atmosphere configuration of the generic ECHAM5 model:

- horizontal resolution = T63
- vertical grid: 47 levels, 26 levels from surface to 100 hPa, top full level = 0.01 hPa

The ocean model MPIOM is used at 1.5 degree resolution with 40 levels. The low top coupled model ECHAM5/MPIOM at resolution T63L31 is identical to the model used for the IPCC-AR4 simulations of the MPI-M.

Experimental design:

Two pairs of experiments are analyzed:

· AMIP experiments: prescribed observed sea surface temperature and ice

o T63L31amip: AMIP experiment with ECHAM5, 1979-1996

o T63L47amip: AMIP experiment with MAECHAM5, 1979-1996

· Coupled experiments: SST and ice simulated, pre-industrial conditions

o T63L31om: experiment with ECHAM5/MPIOM, 100 years

o T63L47om: experiment with MAECHAM5/MPIOM, 100 years

Further the ERA-40 re-analysis is used as a reference dataset. ERA-40 extends to 0.1 hPa, and it has been shown that the ERA-40 (horizontal) circulation and temperature up to 10 hPa is well represented in tropics and extratropics.

Experiments with prescribed sea surface boundary conditions:

Figure 1 shows a comparison of zonal mean temperature in December, January and February (DJF) in the simulations T63L31amip and T63L47amip, and in the ERA-40 re-analysis (Fig. 1, lower right). The bias of the T63L31amip simulation is dominated by a large cold bias in the Northern polar stratosphere of up to -12 K and a warm bias in the tropics and Southern hemisphere near the model top at 10 hPa.

This is a consequence of a biased planetary wave mean-flow interaction in the Northern stratosphere and the related errors in the Brewer Dobson simulation. The lower stratosphere below 30 hPa is generally too cold by about -2 K to -4 K. Further cold biases occur in the extratropical lowermost stratosphere between 100 and 300 hPa in both hemispheres with a maximum error of -8 K and -4 K in the summer and winter hemisphere, respectively. These errors are attributed to too high water vapor mixing ratios, which at these levels induce a too strong radiative longwave cooling. The upper tropical troposphere has a cold bias of -0.5 K to -1 K.

In T63L47amip the stratospheric errors near 10 hPa are much smaller than in T63L31. The large negative error near the North Pole in T63L31amip is replaced by a small positive error of 2 K. Also in the other extratropical areas of the stratosphere the errors are diminished by typically 1 K to 2 K. The upper tropical troposphere is also closer to ERA-40.

The difference between the simulations illustrates the large effects in the temperatures in the Northern extratropical stratosphere (+16 K) and in other latitudes near 10 hPa (~ -2K). Additional significant changes occur in the extratropics between 70 hPa and 300 hPa (+1 K to +2 K) and in the upper tropical troposphere (+0.5 K). Note the generally small differences at the surface where the prescribed SST determines the lower tropospheric temperature efficiently.

The comparison of both AMIP experiments shows significant differences in the atmospheres below 100 hPa. By design this can only be explained by the different representations of the stratosphere. Initial differences in the stratospheric circulation enforce different interactions between the stratosphere and troposphere.

A comparison of the zonal mean zonal wind shows large differences in the stratosphere. Consistent to the strong cold bias near the North Pole T63L31 exposes an exaggerated polar vortex. Differences in the troposphere occur in the upper tropical troposphere and in the extratropics, where zonal winds differ down to the surface.

Coupled atmosphere ocean experiments:

The comparison of the zonal mean zonal temperature in DJF in the coupled experiments shows similar biases in the stratosphere (cf. Fig. 1 and Fig. 2), demonstrating firstly that the coupling to the ocean does not have a significant effect on the major biases near the top of the T63L31 AGCM.

In the troposphere, however, the T63L47 model warms in the coupled experiment almost uniformly by about 0.5 K compared to T63L31, while in the AMIP experiments the temperature differences below 500 hPa were generally small due to the prescribed lower boundary conditions.
Consequently the difference between the zonal mean zonal winds in the tropospheres of the coupled models is different from that between the AMIP models. The differences in the lower troposphere are very small, indicating a difference in the simulated SST of both experiments. Hence the SST must show a response to the initial differences induced by different stratospheric representations. A comparison shows indeed a general warming of the SST in most places by 0.5K. This warming is stronger along the equator in the Pacific, indicating a reduction in the cold tongue bias of the coupled model by 0.5 K to 1 K.
Further preliminary analyses indicate that El Nino is very similar in both models, but that the El Nino teleconnection in surface temperature is better represented in high latitude Eurasia in the high top model.

Summary:

Two pairs of simulations, each with a low and a high top model, have been investigated for effects of different model representations of the atmosphere above 100 hPa on the atmosphere below 100 hPa. It is found that differences in wind and temperature extend from the stratosphere into the troposphere.
The structure and magnitude of these effects depends however on the treatment of the lower boundary condition of the atmosphere. At prescribed lower boundary conditions temperature changes are limited to above 500 hPa, but wind changes extend to the surface. If the atmosphere is coupled to the ocean, the temperature signal spreads almost uniformly in the whole troposphere, but the wind differences are essentially limited to the upper half of the troposphere. Further there are indications that the El Nino teleconnection in surface temperature in Eurasia is better captured in the high top model.

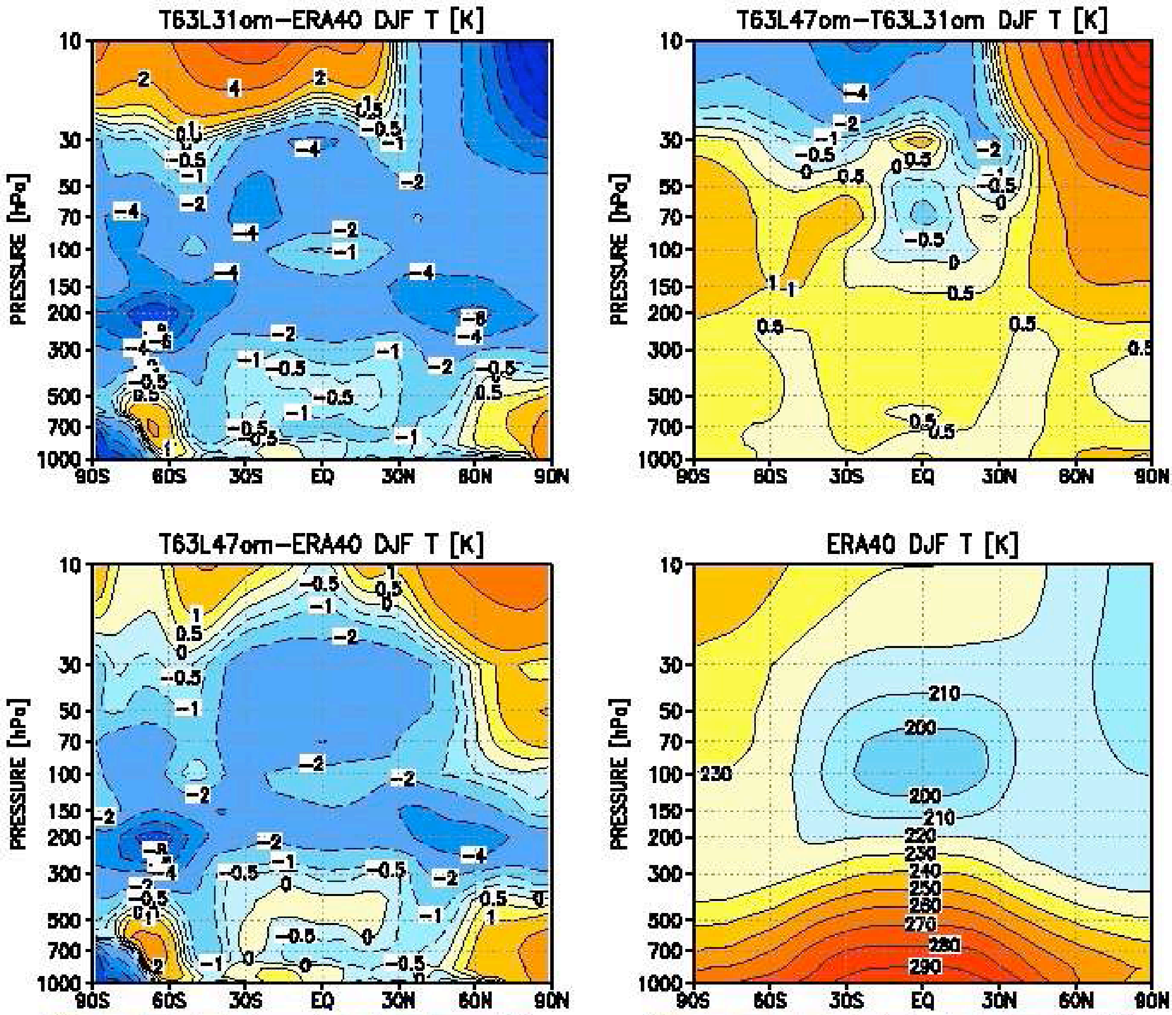

Figure 1: Zonal mean temperature in DJF in ERA-40 (bottom right), difference between T63L31 simulation and ERA-40 (top left) and between T63L47 and ERA-40 (bottom left), and difference between T63L47 and T63L31 (top right).

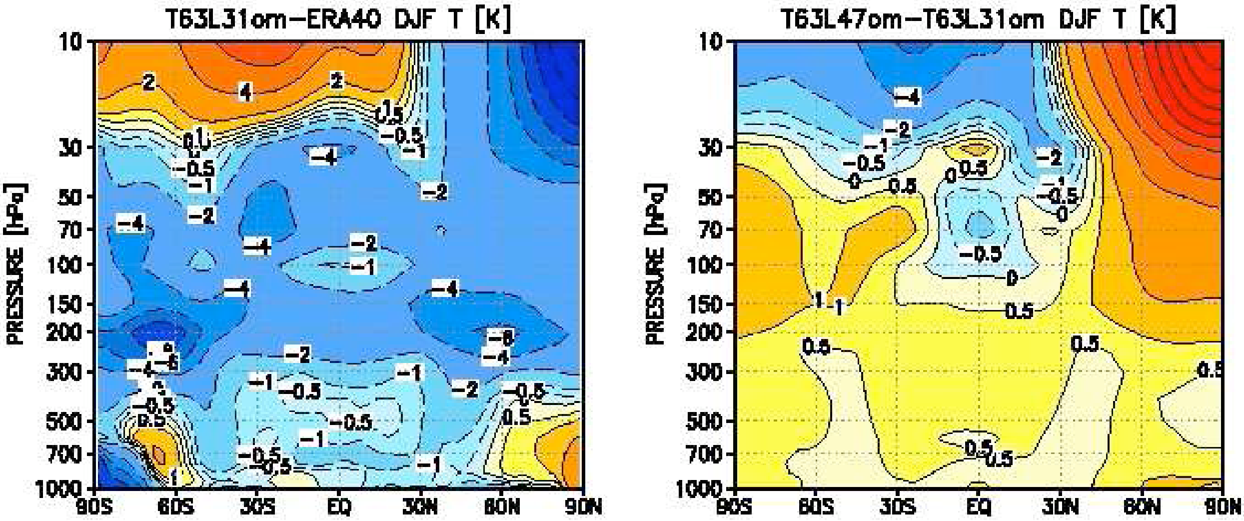

Figure 2: Zonal mean temperature in DJF , difference between T63L31 simulation and ERA-40 (top left) and between T63L47 and ERA-40 (bottom left), and difference between T63L47 and T63L31 (top right).

OPA9 and coupled model

S. Masson[1], G. Madec[1], J.-J. Luo[2], Nemo team, DRAKKAR project team and many others.

1: LOCEAN, Paris, France.
2: Frontier Research Center for Global Change, JAMSTEC, Yokohama, Japan.

This presentation is split in to parts. The first part gives a quick overview of some improvements introduced in OPA 9 whereas the second part show the first results of simulation based on OPA8 or OPA9 (ORCA05L31) coupled to ECHAM5.3 (T106L31).
The majors developments implemented in OPA9 are
Partial steps combined to a new vorticity scheme that conserves energy and enstrophy (named EEN) significantly improve ocean circulation at mid-latitude. In ORCA025, these new physical parameterizations allows us to get realistic features usually reproduced only in much higher resolution simulations. Gulf Stream path is improved. Circulation around the Zapiola dome or along the southern brazilian coast in ORCA025 simulations are comparable (and even better) than some other ocean simulations using 1/10°.
We improved the parameterization of vertical mixing by introducing the impact of the swell on the computation and the surface boundary condition of mixing length. We also add the Langmiur cells as a new source term in TKE equation. These changes mainly improve the mixed layer depth at high latitudes during summer in the ACC region as well as in the north Pacific.
The use of tidal mixing is currently tested in the Indonesian sea. It greatly improves the water mass characteristics along the path and at the mouth of the throughflow.

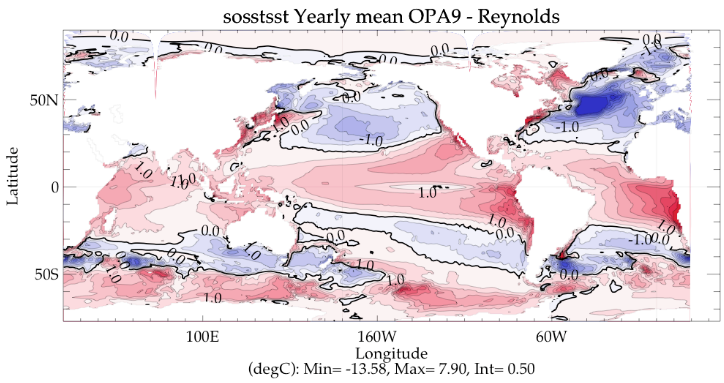

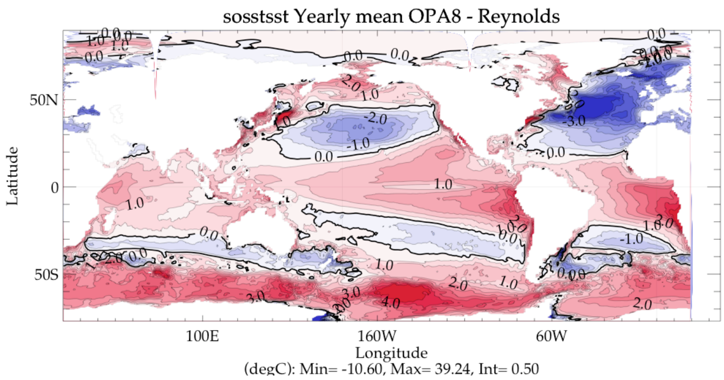

Implementation of AGRIF (Adaptative Grid Refinement in Fortran) has been done and used in forced ocean simulations. This tool allows a 2 ways nesting grids refinement. On going developments will allow to use this tool in a coupled model configuration in a near future.
In addition we also tested several forcing fluxes, advection and vorticity schemes to get the best ORCA05 equatorial dynamics in comparison with TAO mooring. The main results from these tests are, first, wind forcing is a key parameter for the EUC, ERA40 winds are much more suitable than NECP. Second, the new EEN scheme unrealistically slows down the eastern part of the Equatorial Under Current (EUC) and erodes its lower part (which is not the case with ORCA025).

We realized two twin experiments of the coupled model ECHAM with modified versions of OPA8 or OPA9. These version both contain the new TKE and are both not using the partial steps and the new EEN vorticity scheme. However, they are not using the same advection schemes and the sea ice model is used only in the coupling model using OPA9. The results presented are based on the preliminary analyzes of the firsts experiments performed with ECHAM5 coupled to OPA. 50-year long coupled experiments have been perform but results shown are based only on the first 35 years. Both simulations show a global mean warm SST drift of about 1°C during about the first 30 years. Maps of SST difference between experiments climatologies and Reynolds climatology show that the 2 experiments have roughly the same bias (see figure 1). All the major upwelling areas are too warm (from 1° to more than 3°C) and create a global warm bias in the whole tropical ocean. North Pacific and Atlantic are too cold, especially in the area of the Gulf Stream. In the ACC, warm bias in the experiment using OPA9 is reduced in comparison with the other experiment with OPA8. This difference could be explained by the use of sea ice model in the experiment using OPA9.

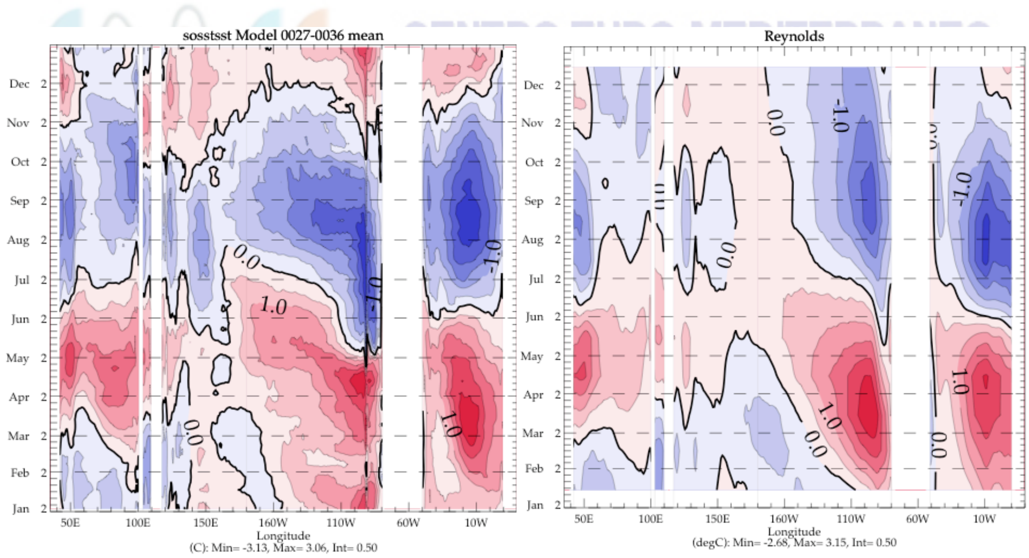

The seasonal cycle of of the pacific equatorial SST is greatly improved in comparison previous version of the coupled model (see figure 2). In agreement with the observations, the eastern Pacific shows a strong annual variability whereas the western Pacific is characterized by a weaker semi-annual variability. In the western equatorial Indian Ocean, the variability is also consistent with the observation. However in the eastern Indian basin, the model variability is unrealistic with an amplitude much larger than the observations. This bias is the signature of the model tendency to produce an IOD every year and is associated to a flat equatorial thermocline that favors the apparition of Sumatra upwelling.

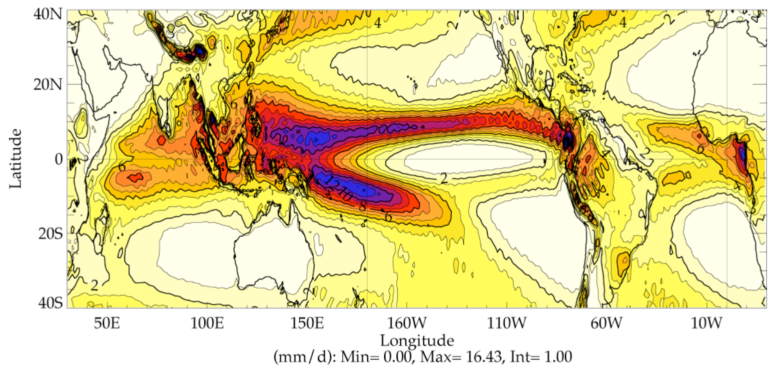

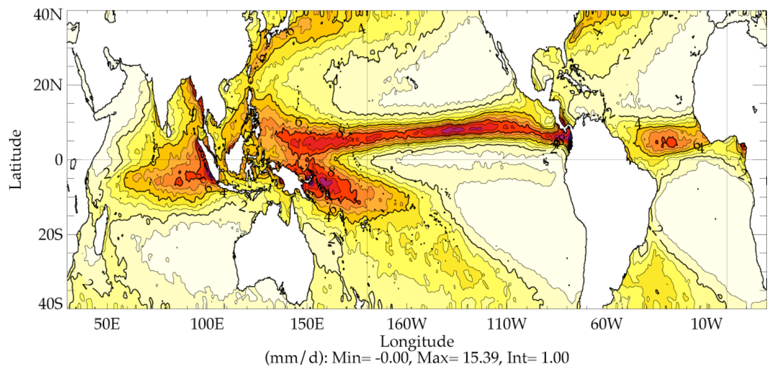

Precipitation of this new coupled experiments using ECHAM5 are also more realistic than results of previous versions of the SINTEX-F coupled model. A double ITCZ is still visible in the tree tropical basins. However its amplitude is much weaker and the SPCZ position improved. Precipitation amplitude is too large in the western Pacific and creates a negative SSS anomaly in the warm pool region.

In the coupled model using OPA9 with the sea ice model, the simulated sea ice extend is realistic in Arctic and slightly too small in Antarctica. The ice thickness show a bias in Arctic with ice accumulation along the coast of siberia.

In conclusion, This new version of the SINTEX-F coupled model show several improvements. Further analyses are ongoing to determine is intraseasonal to interannual variability.